Pergamon

Int. J. Solids Structures Vol. 34, No. 3, pp. 297–326, 1997

0020–7683/97 $15.00 + .00

PII: S0020–9683(96)00021–2

PLASTIC STRESS–STRAIN FIELDS AND LIMIT LOADS OF A PLANE STRAIN CRACKED TENSILE PANEL WITH A MISMATCHED WELDED JOINT

S. HAO, A. CORNEC and K.-H. SCHWALBE
Institute of Materials Research, GKSS Research Centre, Geesthacht, Germany

(*Received* 28 *June* 1995; *in revised form* 20 *December* 1995)

Abstract—The construction of slip-line fields for a centre crack in a tensile panel with a mismatched welded joint will be discussed, from which expressions of the limit load and the constraint state around the crack tip will be derived in an analytical formulation. Based on these solutions the crack driving force of a structure with a cracked mismatched welded joint can be predicted using the procedure of ETM-MM (Engineering Treatment Model, extended for mismatched cracked structures). The theoretical solutions have been verified by 2D finite element calculations. Copyright © 1996 Elsevier Science Ltd.

NOMENCLATURE

γ_{max}^{pl}	maximum plastic shear strain
δ_5	crack tip opening displacement, defined as the displacement of two points at the initial crack tip with 5 mm total gauge length
δ_{5Y}	$\delta_5 = \delta_{5Y}$ when $F = F_Y$ for homogeneous material
δ_{5YL}	$\delta_5 = \delta_{5YL}$ when $F = F_{YL}$ for mismatched CCT
δ_{5YM}	$\delta_5 = \delta_{5YM}$ when $F = F_{YM}$ for mismatched CCT
Δ	displacement at both ends of a CCT panel
β	constant, in plane strain state: $\beta = 6$; in plane stress: $\beta = 2$
ε_{ij}	strain components $(i,j = 1,2)$
θ	angle between an α slip-line and the horizontal direction
φ, r	polar co-ordinates
σ_e	equivalent von Mises stress
σ_{ij}	stress components $(i,j = 1,2,3)$
σ_m	mean stress; in plane strain condition, σ_m equals the triaxial stress
σ_{YB}, σ_{YW}	yield stress of base (B) and weld (W) material, respectively
a	half crack length
k	shear yield stress
n_B, n_W	hardening exponents of base (B) and weld (W) material, respectively
n_{m1}	mismatching hardening exponents at net-section yielding stage
n_{m2}	mismatching hardening exponents at global yielding stage
r, φ	polar coordinates
x_1, x_2	Cartesian coordinates
u_i	displacement components $(i = 1,2)$
v_i	velocity components $(i = 1,2)$
E	elastic modulus
F	applied load for unit thickness
F_Y	limit load for a homogeneous specimen with unit thickness
F_{YL}	the load characterising the beginning of local yielding, per unit thickness
F_{YM}	limit load for a unit thickness cracked tensile panel with a mismatched joint
F_{YW}	limit load for the specimen made of homogeneous weld metal
F_{YB}	limit load for the specimen made of homogeneous base material
H	half height of centred weld metal strip
K_{eff}	effective stress intensity factor, with plastic zone size correction
M	mismatching, $M = \sigma_{YW}/\sigma_{YB}$
Q	constraint parameter at crack tip
T_i	traction force on a body surface
W	half width of CCT panel
CCT	centre crack tension panel
ETM-MM	Engineering Treatment Model for Mismatched Structures
CTOD	crack tip opening displacement.

1. INTRODUCTION

Structures with mismatched welded joints are widely used in engineering application. Here, mismatch means that the weld metal and base material are different in yield stress and in hardening properties. The difference in elastic modulus or Possion's ratio is also possible. But the crack problems of sandwich-like configurations under elastic conditions have already been extensively discussed in the field of composites or interface problems, and for engineering structures, such as bridges, offshore equipment, piping and pressure vessels, the difference in the elastic modulus or Possion's ratio is usually small. Thus, in the present work, we focus on the mismatch problem under elastic–plastic and plane strain conditions.

Generally speaking, an actual welded joint is very complicated, both metallurgically and mechanically. For simplification, in the following analysis the effects of heat affected zones, residual stresses or other kinds of heterogeneity are omitted, and the real welded joint is modelled as a sandwich-like bi-material system as shown in Fig. 1. Both materials have the same elastic modulus and Possion's ratio but the yield stress in the weld material is lower or higher than that in the base material, and this is denoted usually as under- or overmatching, respectively.

For the configuration of Fig. 1, the following questions are of interest:

—How to calculate the crack driving force from elastic to fully plastic condition?
—How to estimate the degree of constraint around the crack tip?

For homogeneous materials several methods (Kumar *et al.* (1931), Dowling and Townley (1975), Schwalbe and Cornec (1991)) are available for estimating the crack driving force. Mismatching may change the monotonicity of the loading process so that under this condition the procedures for homogeneous materials may require alterations. Recently, a substantial body of research work has been reported for the crack problem in mismatched welded joints. For the case that the yield stress of weld metal is far smaller than that in the base material (extreme undermatching), the numerical analysis of Varias *et al.* (1991) has revealed that in small scale yielding conditions the undermatching changes the stress state around a crack tip, as compared to the homogeneous case. A high triaxial stress peak has been observed at a point with a distance of several times the undermatched layer height ahead of the crack tip and a formula for estimating the stress intensity factor has been suggested (Varias *et al.*, 1991). In the field of engineering application, based on the assumption that the J-integral is path-independent, the effect of mismatching on the crack driving force has been investigated by means of finite element analyses within the frame of deformation plasticity theory (Dong and Gordon, 1990, Zhang *et al.*, 1989), and for specimens with various geometries and degrees of mismatching. In the field of experimental determinations of the J-integral, the effect of mismatch on the η-factor for bending specimens

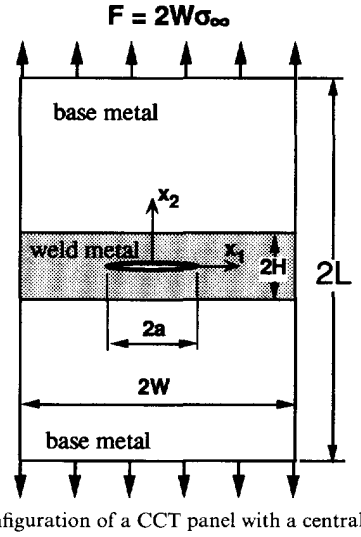

Fig. 1. Configuration of a CCT panel with a central weld strip.

has been studied (Kirk and Dodds, 1992) and a procedure for estimating the J-integral from the measured CMOD has been developed by Gordon and Wang (1993). Combining FE and the slip-line analyses for homogeneous cases the limit load of a bending configuration has been suggested by Joch *et al.* (1993). A slip-line analysis for CCT configuration with an undermatched welded joint has been carried out by Hao *et al.* (1991). Experimental work in this field has also been reported. For example, the fracture behaviour of various structures with cracked mismatched welded joints, in which the location and orientation of the crack are different, has been investigated (Koçak *et al.*, 1988, 1990, Petrovski and Koçak, 1994, Denys, 1991, Toyoda *et al.*, 1994, Thaulow *et al.*, 1994). All results demonstrate that both the degree of mismatching and the geometrical parameters, such as weld strip height and crack location, have strong effects on the behaviour of the crack driving force and the fracture resistance. Since many different parameters are involved in the mismatch problem, research work is usually performed case by case for given material properties and geometry. However, for engineering application a more general solution is needed, based on methods such as those (Kumar *et al.*, 1981, Dowling and Townley, 1975, Schwalbe and Cornec, 1991) derived for homogeneous materials. With this aim, the authors' research group has carried out a comprehensive experimental (Koçak *et al.*, 1988) and analytical research program (Hao *et al.*, 1991).

Basic studies of mismatch effects are often performed on tensile loaded plates containing a welded joint, but actually this welded joint is idealised as a homogeneous strip, as depicted in Fig. 1. For the homogeneous case the analysis is as follows: when the load is below the limit load of the structure, the elastic analysis with a small-scale yielding modification is used; when the load level is beyond the limit load, the post-yield analysis is used according to the hardening property of the material. As a transition point, the limit load represents the end of the small-scale yielding state and governs the crack behaviour in the post-yielding region. For homogeneous materials, a number of limit load solutions for various geometric configurations have been derived using the plastic slip-line theory. No such solutions have been reported so far for heterogeneous cases. This is because the slip-line theory has been derived for homogeneous conditions; furthermore, the physical meaning of a "limit load" for a heterogeneous material still has to be defined.

A series of finite element analysis (Hao *et al.*, 1994a, 1994b, 1994c) have been performed for the configuration shown in Fig. 1, which is in relation to the work reported in the present paper. A typical example of the crack driving force curve is shown as the solid points in Fig. 2, from which one can clearly see that there is an explicit "turn point" between the local yielding and net-section yielding region. The physical meaning of the load level at this "turn point" is "limit load", symbolising the onset of net-section yielding.

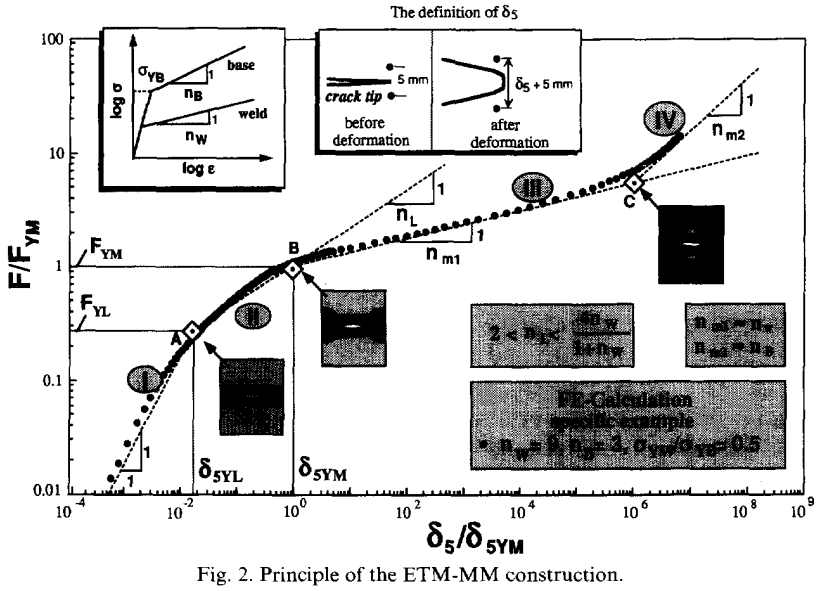

Fig. 2. Principle of the ETM-MM construction.

In fact, in the middle strip in Fig. 1, we may assume that there is no deformation in the base material if the yield stress of the base material is so high that the plastic strain is totally confined to the weld metal strip. Then the cracked mismatched structure shown in Fig. 1 is actually modelled as a mechanical problem of a centre crack in a strip embedded in a rigid surrounding, which is resolvable analytically by the slip-line theory. If the difference of the yield stresses is only moderate and the plastic deformation is distributed over both materials, it is also possible to derive exact or approximate limit load solutions by using the classical plastic upper- and lower bound theory, with the support of additional finite element analysis. These are the main tasks that will be discussed in the present work.

The Engineering Treatment Model (ETM) has been developed for assessing the integrity of structures made of homogeneous materials (Schwalbe and Cornec, 1991). Its extension, ETM-MM, serves for estimating the crack driving force in mismatched welded joints (Schwalbe, 1992, Schwalbe *et al.*, 1994, Hao *et al.*, 1994a, 1994d). The structure of the crack driving force for mismatched conditions can be demonstrated by means of the example shown in Fig. 2, where the crack-tip opening displacement δ_5 is considered as the crack driving force. Our previous work (Hao *et al.*, 1994a, 1994b, 1994c) has shown that the load vs δ_5 relationship can be divided into four different sections forming the elements of the ETM-MM (see Fig. 2):

Stage I (small scale yielding): $F \leqslant F_{YL}$

$$\delta_5 = \frac{K_{eff}}{E\sigma_{YW}}[\eta_1 K_{eff} + \eta_2] \quad \text{with } \eta_1 = 0.4\pi\kappa_1\kappa_2; \quad \eta_2 = \kappa_1\sigma_{YW}\sqrt{l} \tag{1a}$$

where $l = 2.5$ mm;

$$\kappa_1 = \frac{F_{Y,\text{weld}}}{0.9F_{YM}}; \quad \kappa_2 = 2 - \frac{\pi}{2+\beta}\sin\left(\frac{\pi a}{W}\right); \quad \beta = \begin{cases} 2 \text{ plane stress} \\ 6 \text{ plane strain} \end{cases}$$

Stage II (local yield): $F_{YL} \leqslant F \leqslant F_{YM}$

$$\frac{\delta_5}{\delta_{5YL}} = \left[\frac{F}{F_{YL}}\right]^{n_L} \quad \delta_{5YL} = \frac{K_{eff}(F_{YL})}{E\sigma_{YW}}[\eta_1 K_{eff}(F_{YL}) + \eta_2]$$

$$n_L = \frac{4n_W}{1+n_W} \tag{1b}$$

Stage III (net section yielding): $F_{YM} \leqslant F$

$$\frac{\delta_5}{\delta_{5YM}} = \left[\frac{F}{F_{YM}}\right]^{n_{m1}} \quad \delta_{5YM} = \delta_{5YL}\left[\frac{F_{YM}}{F_{YL}}\right]^{n_L} \tag{1c}$$

State IV (gross section yielding): This area will not be considered in this paper.

In eqns (1a–c), F_{YM} represents the net section yield load and F_{YL} the local yield load, $= \kappa F_{YM}$, with $\kappa \approx 0.5$–0.9 depending on geometry and material properties (Hao *et al.*, 1991, Hao *et al.*, 1994b, 1994c), n_{m1} is the hardening exponent characterizing the net section yielding behaviour (Schwalbe *et al.*, 1994) and E, n_W, σ_{YW} and K_{eff} denote the elastic modulus, the hardening exponent and the yield stress of the weld metal, and the effective stress intensity factor, respectively.

By eqns (1a–c), one can determine the crack driving force of a structure with mismatched welded joint if the limit load and material properties are known. In the present work we focus on the determination of the limit load, based on the slip-line analysis of the mismatched CCT tensile panel as shown in Fig. 1.

On the other hand, mismatch does not only change the limit load and crack driving force, it may also have strong effects on the material's fracture behaviour. This is because

mismatching may alter the stress–strain distribution around a crack tip; different stress–strain fields may lead to different constraint conditions, which may change the ductile-to-brittle transition temperature of the structure (Schwalbe *et al.*, 1994, Kirk *et al.*, 1991). Therefore, the condition of constraint at the crack tip is significant for the fracture behaviour, and establishing the relationship between geometry, constraint state, load, and material properties is highly required for engineering applications.

In the present work, the stress–strain field and the constraint conditions of a crack in a CCT configuration with a centred mismatched welded joint will be investigated, with particular emphasis on the effects of geometry and degree of mismatching. Based on the slip-line solutions we will estimate the constraint state around the crack tip, the limit load as well as the crack driving force in a mismatched structure. In the following section we will focus first on the case of extreme undermatching. The general solution for the limit load for undermatching will be discussed in the third section. The case of overmatching will be shown subsequently. Several analytical expressions for the constraint state at a crack tip have been obtained and the discussion of the constraint problem for mismatch will be presented in the fifth section. All theoretical results have been verified by finite element analyses. Two-dimensional finite element calculations were performed for the configuration of Fig. 1 with the a/W ratio varying from 0.05 to 0.8 and the H/a ratio from 0.125 to 3 under plane strain condition. A typical finite element mesh is shown in Fig. 3. The finite element analyses were done using the finite element code ABAQUS on IBM workstations. The results obtained will be briefly discussed in each section.

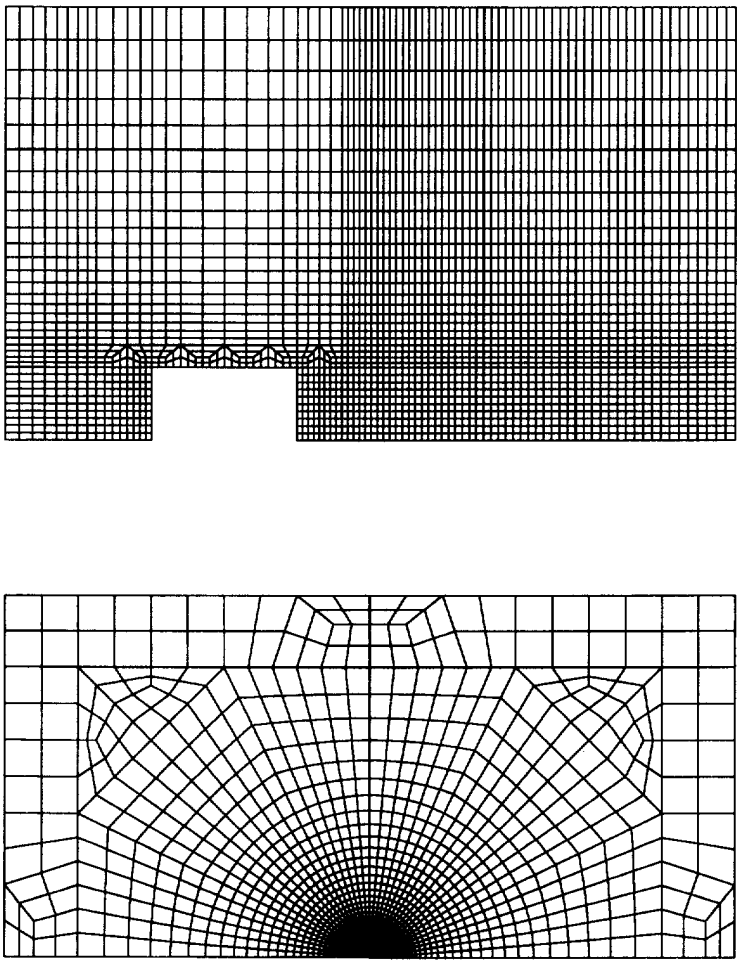

Fig. 3. Finite element mesh of the CCT.

2. SLIP-LINE FIELDS FOR EXTREME UNDERMATCHING

First we define the mismatch factor M

$$M = \frac{\sigma_{YW}}{\sigma_{YB}} \tag{2}$$

where σ_{YW}, σ_{YB} denote the yield stress of weld metal and base material, respectively.

As mentioned in the previous section, when $M \ll 1$, only the weld metal strip deforms plastically. For this "extreme undermatching" condition we assume:

1. the base material is rigid;
2. the weld metal is rigid-perfectly plastic, obeying von-Mises yield criterion;
3. the thickness of the panel is large enough to maintain plane strain condition.

Thus, the slip-line field analysis of the general problem in Fig. 1 is simplified as a finite width strip with a centre crack under a rigid displacement boundary extension in the plane strain condition, which can mathematically be expressed as:

$$\text{at} \quad x_2 = \pm H: \quad \text{when } \sigma_{12} < k \quad u_2 = \pm\Delta, \quad u_1 = 0$$

$$\text{when } \sigma_{12} = k \quad u_2 = \pm\Delta \quad u_1|_{x_2=H+0} \neq u_1|_{x_2=H-0} \tag{3a}$$

$$\text{at} \quad x_2 = \pm 0 \quad \text{and} \quad -a \leqslant x_1 \leqslant a: \quad \sigma_{22} = \sigma_{12} = 0$$

$$x_1 = \pm W: \quad \sigma_{11} = \sigma_{12} = 0 \tag{3b}$$

$$\varepsilon_{13} = \varepsilon_{23} = \varepsilon_{33} = 0 \tag{3c}$$

where y, σ and ε denote displacement, stress and strain components, respectively, the subscripts 1, 2, 3 denote the component in the corresponding co-ordinate directions; Δ represents the rigid displacement extension or the rigid displacement of the base material, k is the shear yield stress.

The plastic flow in this situation can be classified as a non-steady motion problem in two dimensions according to the classical theory of plasticity (Hill, 1951) and the slip-line analysis is applicable. Obviously, the ratio $(W-a)/H$ is an important parameter for constructing the slip-line field. First we investigate the two extreme cases with the ratio $(W-a)/H$ being very large or very small.

Case 1: $(W-a)/H < 1$

In this case the slip line (shear band) begins at the crack tip and stretches to the traction-free side boundary with 45 degrees declined to the horizontal axis, Fig. 4(a). There is no additional constraint effect from the base material so that this slip-line field is exactly the same as in the case of a CCT consisting of homogeneous weld material.

Case 2: $(W-a)/H \gg 1$

If we change the sign of the upper and lower boundary displacements in eqn (3a), we obtain another typical classical problem in plastic slip-line theory: the compression of a perfectly plastic block between rough rigid plates, which has been investigated by Prandtl (1923) and Prager (1953). For this problem Prandtl (1923) has deduced the slip-line field in an approximate way as shown in Fig. 5a, in which the corresponding slip lines are identical cycloids. Prager (1953) has shown that if the ratio W/H (see Fig. 5(a)) is large enough this result is close to the numerical solution obtained by means of finite differential method.

Enlightened by the above mentioned Prandtl solution, we may change the sign of the field in Fig. 5(a) to obtain a slip-line field for a centred crack in the weld metal strip under tension (Hao *et al.*, 1991) (Fig. 5(b)). Obviously, it offers a displacement compatible field, and the equilibrium condition in this field has been satisfied as the two groups of identical cycloids are normal to each other. But if one checks the stress level in the rigid zone near

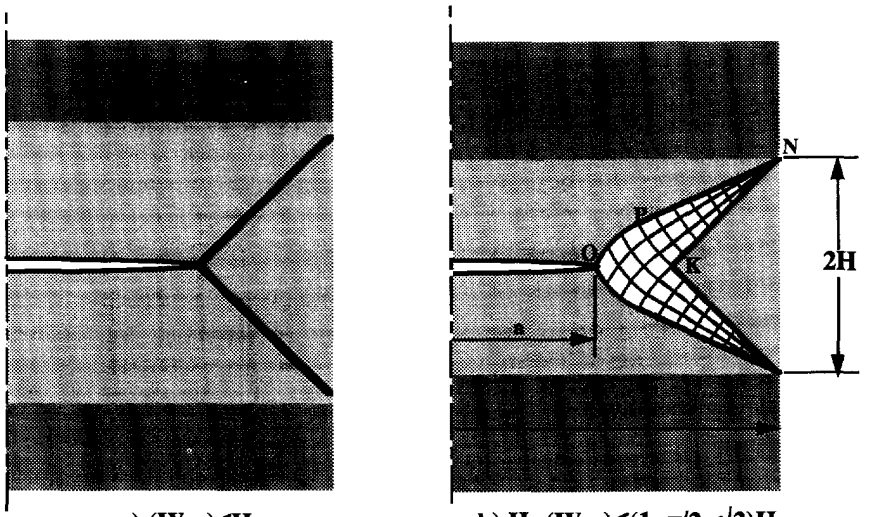

a) (W-a)≤H

b) H<(W-a)≤(1+π/2+√2)H

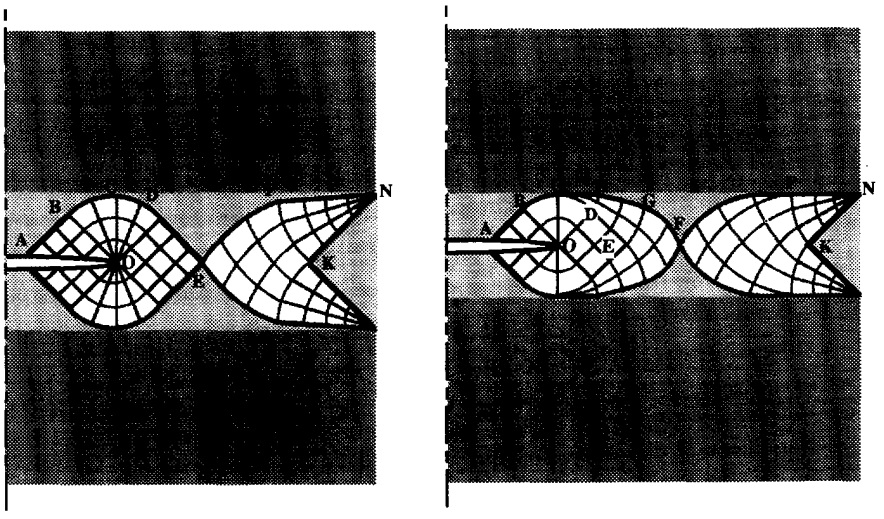

c) (1+π/2+√2)H<(W-a)≤(1+π/2+2√2)H

d) (1+π/2+2√2)H≤(W-a)<(3.88+2π+√2)H

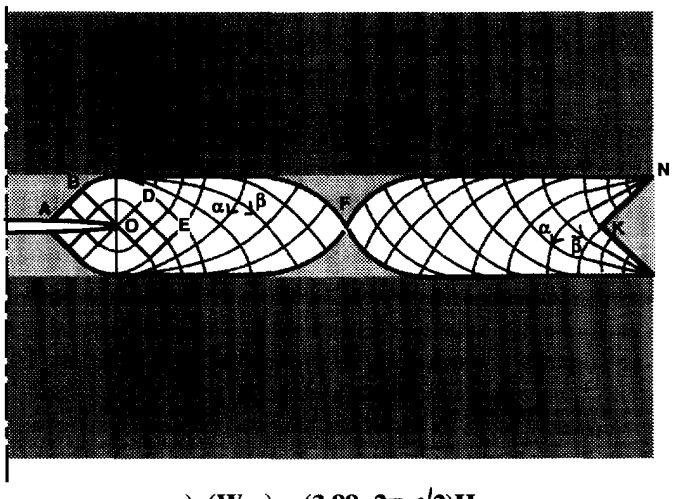

e) (W-a) > (3.88+2π+√2)H

Fig. 4. Slip-line fields for varying $(W-a)/H$ ratios for extreme undermatching.

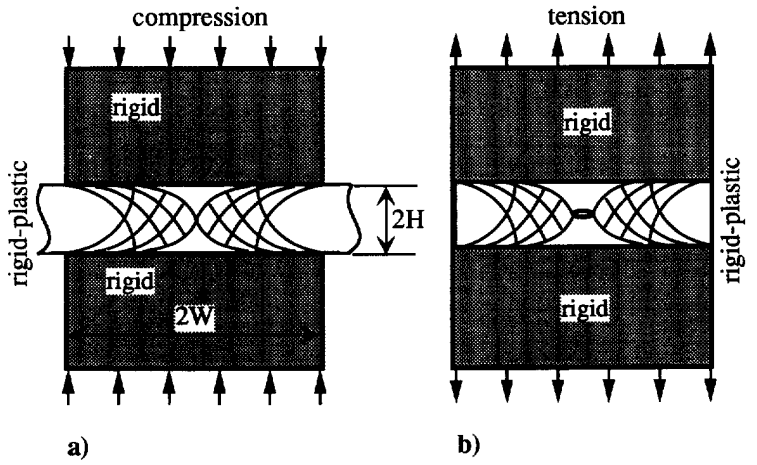

Fig. 5. (a) The Prandtl solution for the compression loaded rigid block with rough surfaces on a perfectly rigid-plastic material. (b) First approximate solution of a slip-line field for extreme undermatching conditions.

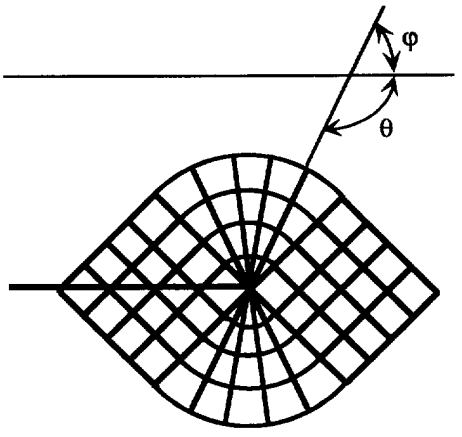

Fig. 6. Prandtl field at the crack tip.

the crack tip carefully, one finds that the equivalent stress in this area is higher than the yield stress, so that this slip-line solution is only a rough estimate and it would lead to a overestimated limit load as the yielding condition is not satisfied in the rigid zone.

Under small scale yielding conditions for a homogeneous medium, it has been demonstrated (Hutchinson 1968) that for perfectly plastic materials there is another kind of slip-line field around a crack tip as shown in Fig. 6, which was also deduced by Prandtl and is commonly named a Prandtl field. But in a homogeneous tensile panel the size of the Prandtl field is usually very small and its validity is restricted to the immediate vicinity of the crack tip. This is because the Prandtl field may exist only under the condition of high constraint resulting from the elastic surrounding zone. In the elastic–plastic or fully plastic condition, other slip-line fields such as the type in Fig. 4(a) may govern the crack tip, as the plastic zone has already expanded to the traction-free boundary edge and the high constraint state around the crack tip has been relaxed.

However, for the case shown in Fig. 1 with large $(W-a)/H$ ratio, the strain gradient from the crack tip to the traction-free edge is larger than that in the homogeneous case even if the panel is under fully plastic condition. This is because, due to the extra constraint of the base material on the slender centred strip, the resistance against plastic flow is remarkably elevated. Therefore we may assume that under this situation the Prandtl field may exist at the crack tip, and it may expand further and dominate a large area around the crack tip even under fully plastic condition. The accompanied finite element results confirm this assumption and will be shown later. Starting from the solutions in Figs 5(b) and 6,

the slip-line fields under plane strain condition for the extremely undermatched CCT configuration with the ratio $(W-a)/H > 1$ have been reconstructed as shown in Fig. 4 (b–e), from which one may obtain the entire set of solution of plastic flow, limit load and the stress distribution in the plastic zone.

Figures 4(c, d, e) are for the case of $(W-a)/H \gg 1$, in which the Prandtl field begins at the crack tip and expands to the border of the weld strip, thus the traction-free boundary condition at the crack surface is satisfied. Towards the ligament the Prandtl field evolves into the field CDEGH (Fig. 4(d, e)) in which one group of slip lines in the area of DEGH are straight lines, for example, the lines HG or DE. On the traction-free edge of the ligament, there is a fan-shaped field KNP centred at the end of the interface between base material and weld metal. By using the procedure introduced by Hill (1951) and Dewhurst and Collins (1973), it is not difficult to deduce the numerical solution of the slip-line field in the ligament according to the boundary conditions supplied by the field CDEGH at one side and the fan-shaped field KNP at the other side. When $(W-a)/H$ is not small, there is a slip-line field constructed by two orthogonal cycloid families at the middle, which is the same as the field in Fig. 5(a), and at two sides it connects with another two fields but with unknown transition fields somewhere in-between.

It should be noted, however, that the transition fields between the different basic slip-line fields can be omitted and it can be simply assumed that the cycloid field joins directly the field CDEGH at one side and the fan-shaped field KNP at the other side. In this case the continuity condition for the remaining slip-line fields is not exactly satisfied but our analysis indicates that the difference in stresses is less than 5% (see Appendix 2).

On the centre line of the weld strip the orthogonal cycloid fields develop from both sides and at the point F they join together (see, for example, Fig. 4(e)). With decreasing ratio $(W-a)/H$ the cycloid field at the left side of point F degenerates (see Figs 4(d), 4(c), 4(b), 4(a), sequentially). From the slip-line fields in these figures the stress distribution and limit load can be determined analytically. Because of the limitation of the paper length, we introduce only the details of the case shown in Fig. 4(e) as follows.

First we consider the stress distribution in the Prandtl field around the crack tip. Starting from the fraction-free crack region, denoted ABO in Fig. 4(e), in this region the yield criterion and the free surface require that the stress field is a homogeneous tensile (or possibly compression) field parallel to the crack flanks:

$$\sigma_{11} = 2k, \quad \sigma_{22} = 0, \quad \sigma_m = k \tag{4a}$$

where σ_m represents the mean stress, i.e., the triaxial stress, which is equal to σ_{33} for the incompressible material under plane strain condition.

The stress components in the fan shape region OBCD are

$$\sigma_m = k\left(1-\frac{\pi}{2}-2\theta\right)$$

$$\sigma_{11} = \sigma_m - k\sin 2\theta, \quad \sigma_{22} = \sigma_m + k\sin 2\theta, \quad \sigma_{12} = k\cos 2\theta \tag{4b}$$

where θ is the angle between the x_1 axis and the tangent direction of the α group slip-lines. In this fan shape zone $\theta = \varphi - \pi$. For example, for the α line DO $\varphi = \pi/4$, so $\theta = -3\pi/4$. Then in the region ahead of the crack tip, denoted as ODE in Fig. 4(e), the stress system consists of the simple stress state

$$\sigma_{11} = k\pi, \quad \sigma_{22} = k(2+\pi), \quad \sigma_m = k(1+\pi), \sigma_{12} = 0. \tag{4c}$$

The zone CDEGH is out of the Prandtl field and there is no closed slip-line formulation like eqns (4(a–c)) available. By means of the method introduced in Hill (1951), Dewhurst and Collins (1973) we have obtained a numerical solution which is listed briefly in the Appendix 1. However, the stress distribution in this area does not have much influence on the limit load and on the constraint state at the crack tip.

The cycloid field EGF is part of the basis slip-line solution of Fig. 5(a), and in the co-ordinate system $\{x_1, x_2\}$ centred at the crack tip the stress components are:

$$\sigma_{11} = k\left(2-\sqrt{2}+\pi+\frac{x_1}{H}-2\sqrt{1-\left(\frac{x_2}{H}\right)^2}\right)$$

$$\sigma_{22} = k\left(2-\sqrt{2}+\pi+\frac{x_1}{H}\right)$$

$$\sigma_{12} = -k\left(\frac{x_2}{H}\right)$$

$$\sigma_m = k\left(2-\sqrt{2}+\pi+\frac{x_1}{H}-\sqrt{1-\left(\frac{x_2}{H}\right)^2}\right). \tag{4d}$$

Similarly, the stress distribution in the cycloid field FKP is

$$\sigma_{11} = k\left(C_5-\frac{x_1}{H}-2\sqrt{1-\left(\frac{x_2}{H}\right)^2}\right)$$

$$\sigma_{22} = k\left(C_5-\frac{x_1}{H}\right)$$

$$\sigma_{12} = -k\left(\frac{x_2}{H}\right)$$

$$\sigma_m = k\left(C_5-\frac{x_1}{H}-\sqrt{1-\left(\frac{x_2}{H}\right)^2}\right). \tag{4e}$$

The position of point F and the constant C_5 in eqn (4e) are yet unknown. According to the traction-free boundary condition at the plate's edge and the joint condition with the field EGF at the point F we have:

$$\text{in eqn (4e):}\quad C_5 = 1+\frac{W-a}{H}$$

$$\text{at point F:}\quad x_1|_F = \tfrac{1}{2}[W-a+H(\sqrt{2}-1-\pi)]. \tag{4f}$$

From eqn (4d) it can be seen that with increasing the value of the x_1 co-ordinate the stress components σ_{11}, σ_{22} as well the triaxial stress σ_m are elevated linearly, which can be explained as the consequence of the high constraint of the base material.

Finally we deal with the fan-shape like field KNP. In this field the stress distribution is

$$\sigma_m = k\left(1-2\theta-\frac{3\pi}{2}\right)$$

$$\sigma_{11} = \sigma_m - k\sin 2\theta,\quad \sigma_{22} = \sigma_m + k\sin 2\theta,\quad \sigma_{12} = k\cos 2\theta \tag{4g}$$

which satisfies the traction-free condition at the panel's edge and the stress connection condition on the curve KP approximately without regard to the transition zone. In this case the maximum error in the stress is less than 3% and further details of it are described in Appendix 2.

Using the stress distribution just derived, the limit load is now given by

$$F_{YM} = \int_{OE} \sigma_{22}\,dx_1 + \int_{EF} \sigma_{22}\,dx_1 + \int_{FK} \sigma_{22}\,dx_1 + \int_{KN} \sigma_{22}\,dx_1 + \int_{KN} \sigma_{12}\,dx_2. \tag{5}$$

Up to now we have deduced the complete stress distribution in the weld strip shown in Fig. 4(e). By varying the ratio $(W-a)/H$ and the mismatch factor M the slip-line field varies also. For extreme undermatching cases, with decreasing ratio $(W-a)/H$, the cycloid fields at both sides of the point F shrink and finally degenerate. The corresponding slip-line fields have also been derived and are shown in Figs 4(d), 4(c), 4(b), 4(a). Using the same analysis procedure as for Fig. 4(e) the stress distribution and limit load can easily be determined analytically for the other cases. The related expressions for the limit load will be listed in Appendix 1.

To verify the slip-line fields derived above, a corresponding finite element analysis has been performed, in which the contours of the maximum plastic shear strain are calculated. The results match perfectly the slip-line field analysis in Figs 4(c–e).

Figure 7 displays the distributions of the stress components calculated from the slip-line solutions (e.g. eqns 4a–4g) along the middle line of the ligament in the weld metal. In this diagram for the case $(W-a)/H = 14$ the peak point of stress components is the point F in Fig. 4(e). From eqns 4d–4e one can find also that in the slip-line fields EGF and FKP the stress σ_{22} is independent of the x_2 co-ordinate, which means: the maximum principal stress remains a constant in the transverse direction of the weld metal. At the centre line of the weld strip ($x_2 = 0$) there is always $\sigma_{22} = \sigma_{11} + 2k$. With increasing the value of the x_2 co-ordinate σ_{22} remains constant but σ_{11} increases. At $x_2 = H$ (on the interface) σ_{11} has the same value as σ_{22} and σ_m. In the numerical work of composite materials this phenomenon has also been observed (Varias *et al.*, 1991). Using the slip-line analysis (eqns (4a–f)) we can calculate the value of the stress peak and its position exactly.

Figures (8a) and (b) illustrate the distribution of stress components around the crack tip as determined from the finite element calculations, corresponding to the case in Fig. 4(d). It is noteworthy that the distribution in Fig. 8(a) is almost exactly identical to that predicted by the Prandtl field. This result proves that the assumption suggested above is realistic for undermatching, i.e., the Prandtl field does not only exist under small-scale yielding state, under the extremely undermatching condition it may enlarge with loading, until the load reaches the limit load and the panel exhibits a fully plastic state.

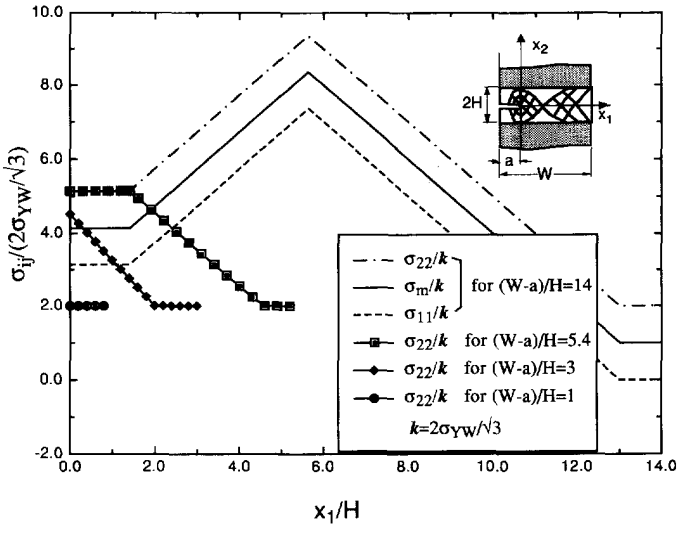

Fig. 7. Stress distribution from the slip-line fields along the middle line of ligament in weld metal for varying $(W-a)/H$.

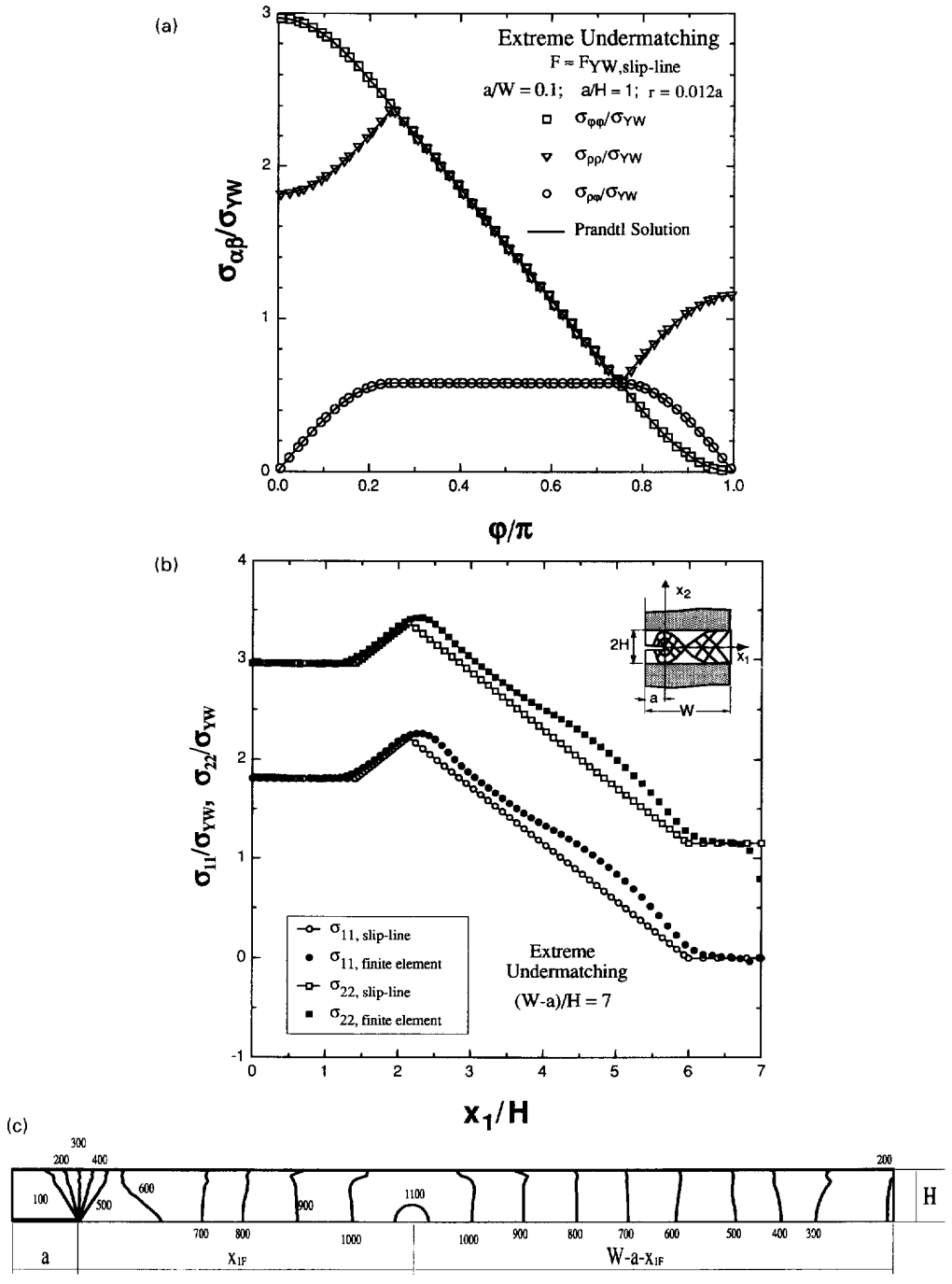

Fig. 8. (a) Stress distribution from the slip-line field around the crack tip at a fixed distance and the comparison with the finite element calculation for the case of Fig. 4d. (b) Stress distribution from the slip-line field on the ligament ($x_2 = 0$) ahead of the crack tip and the comparison with the finite element calculation, for the case of Fig. 4d. (c) Contours of the stress distribution σ_{22} in the weld metal strip.

Figure 8(b) illustrates the comparison of stress distributions on the ligament, which are determined by the slip-line solution (Fig. 4(d)) and by the finite element analysis, respectively. Both techniques yield very similar results. The differences come partly from the omitted transition fields between the different slip-line fields and perhaps from the additional elastic constraint, as the slip-line analysis is based on the rigid-perfect plasticity law and the numerical result (Varias *et al.*, 1991) indicates that the elastic material properties may cause the deviation of the stress distribution.

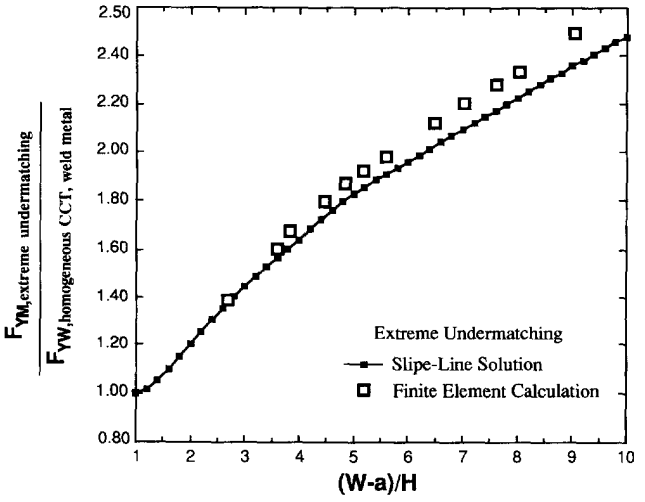

Fig. 9. Comparison of the limit load derived from the slip-line solution and finite element results for extreme undermatching condition.

It is noteworthy that in Fig. 8(b) the maximum stress occurs at a point with a certain distance away from the crack tip. The value of this stress peak is far higher than that at the crack tip. This is because due to the geometrical constraint from the strong base material the resistance to plastic flow in the weld metal increases so remarkably that a high triaxial stress develops in the middle area of the ligament. Using eqns (4(a–e)) the complete stress distributions, for example, the value of the peak stress and its position are already determined analytically. Figure 8(c) shows the isolines of σ_{22} in the weld strip ahead of a crack tip. Comparing them with Fig. 4(e) it can be seen clearly that at the point F the stress reaches its maximum value and in the zones within slip-lines σ_{22} is almost independent of the x_2 co-ordinate, as indicated by eqns (4(d–e)). Further details of the slip-line systems presented are described in Appendices 1 and 2.

Figure 9 shows the comparison of the theoretical prediction of the limit load by eqn (5) with the finite element results. It can be seen that extreme undermatching leads to a significant increase of the limit load as compared to the case of a CCT made of homogeneous metal. This conclusion coincides with the stress distribution shown in Fig. 8(a), because in the area with strong hydrostatic stress a higher load is needed to reach the global yield condition.

From previous analysis it is clear that for mismatching cases the effect of geometry is important since the different geometric parameters cause different degrees of global constraint, which correspond to distinct deformation models. The CCT configuration with a through-crack under plane strain condition is often used as a typical case study for fracture analysis. Further work on 3D conditions and on a surface crack problem (Hao *et al.*, 1994b, 1994c) have indicated that the solutions of plane strain mismatch CCT configuration provide a fundamental basis for other geometries and have widespread significance for application.

3. GENERAL EXPRESSION OF THE LIMIT LOAD FOR UNDERMATCHED TENSION STRUCTURES

The solutions discussed in the previous section have been derived under the assumption that the base material is rigid or deforms only elastically so that the plastic deformation is always confined to the weld metal, which represents extreme undermatching. If the base material deforms plastically but the mismatch in yield stress, expressed by the factor $M = (\sigma_{YW}/\sigma_{YB})$, is very small, the *extreme undermatching* condition can also hold so that the slip-line solutions obtained previously are still correct. However, if the ratio M is no longer very small, but still smaller than unity, i.e., undermatching is still present, the plastic deformation may extend from the weld strip into the base material as the latter is not strong

enough to keep the high constraint state for extreme undermatching. For application, the following two questions are then of interest:

(i) What is the slip-line field for a structure with only a slight undermatching (M close to 1)?
(ii) What is the maximum value of M at the point, where the extreme undermatching condition is no longer valid?

To answer the first question the slip-line field shown in Fig. 10(a) has been constructed, hereafter referred to as the *penetrating slip-line solution* for a CCT configuration. Obviously it is a kinematically compatible field so that it may lead to an "upper bound solution" of the limit load (Hill, 1951). The angle ϕ and the stress distribution along the slip line are to be determined. According to the traction-free edge of the plate the angle ϕ must equal 45 degrees. Assuming that there is a local stress jump on the slip-line at the interface of the two materials then in both materials the yielding condition can be satisfied. The distribution of this jump is described in Appendix 4. A more general discussion of the slip-line field in a bi-material has been given in Hao *et al.* (1994b). The expression of the limit load for slight undermatching is

$$F_{YM,\text{penetrating slip-line}} = \frac{4\sigma_{YW}}{\sqrt{3}}\left[H + \frac{W-a-H}{M}\right] \quad \text{valid for} \frac{W-a}{H} \geqslant 1. \tag{6}$$

This expression will be discussed in Appendix 3.

Figure 10(b) shows the contour of maximum shear strain from finite element calculation for slight undermatching with $M = 0.66$. The plastic zone spreads through both materials like the situation of a homogeneous CCT. Figure 11 compares the limit load from the finite element analysis and calculated by eqn (6). Both methods yield very similar results. These results confirm that the penetrating slip-line field illustrated in Fig. 10(a) is mechanically reasonable for the cases in which the yielding is not confined to the weld strip.

Thus, for a CCT specimen with undermatching weldment, there are two possible deformation fields: the penetrating slip-line field or the slip-line field confined to the weld metal as shown in Figs 4(a)–4(e), from which we can obtain two different limit loads. In the following we will focus on the question: which solution is the realistic one?

It is clear that both kinds of the slip-line fields are kinematically compatible displacement fields. In a kinematically compatible field the displacement boundary condition and the incompressible condition are always satisfied, but the equilibrium equation or the yield condition or the force boundary condition may not be satisfied somewhat in the structure. From the basic variational principle in the classical theory of plasticity (Hill, 1951, Koiter, 1960), it is well known that for a rigid-perfectly plastic material any kinematically compatible field leads to an upper-bound solution. This "upper bound theorem" can be extended to the bi-materials cases if there is no debonding on the interface. Therefore for the mismatching problem, we deduce the lemma as follows.

For the undermatched CCT specimen as shown in Fig. 1, the slip-line solution, which leads to a lower limit load, is closer to the true solution than other slip-line fields with higher limit loads.

Therefore we define the limit load ratio R:

$$R = \frac{F_{YM,\text{penetrating slip-line}}}{F_{YM,\text{weld strip-line}}}. \tag{7}$$

From the lemma mentioned above we can draw the conclusion that for $R < 1$ the penetrating slip-line solution is relevant whereas for $R > 1$ the slip-line confined in the weld strip is valid.

Figure 12 illustrates the dependence of the ratio R on the geometric parameters and the degree of mismatch. Figure 13 gives an overview of the limit load behaviour of the mismatched CCT with different H/W ratios and $M = 0.5$, as compared with the CCT made

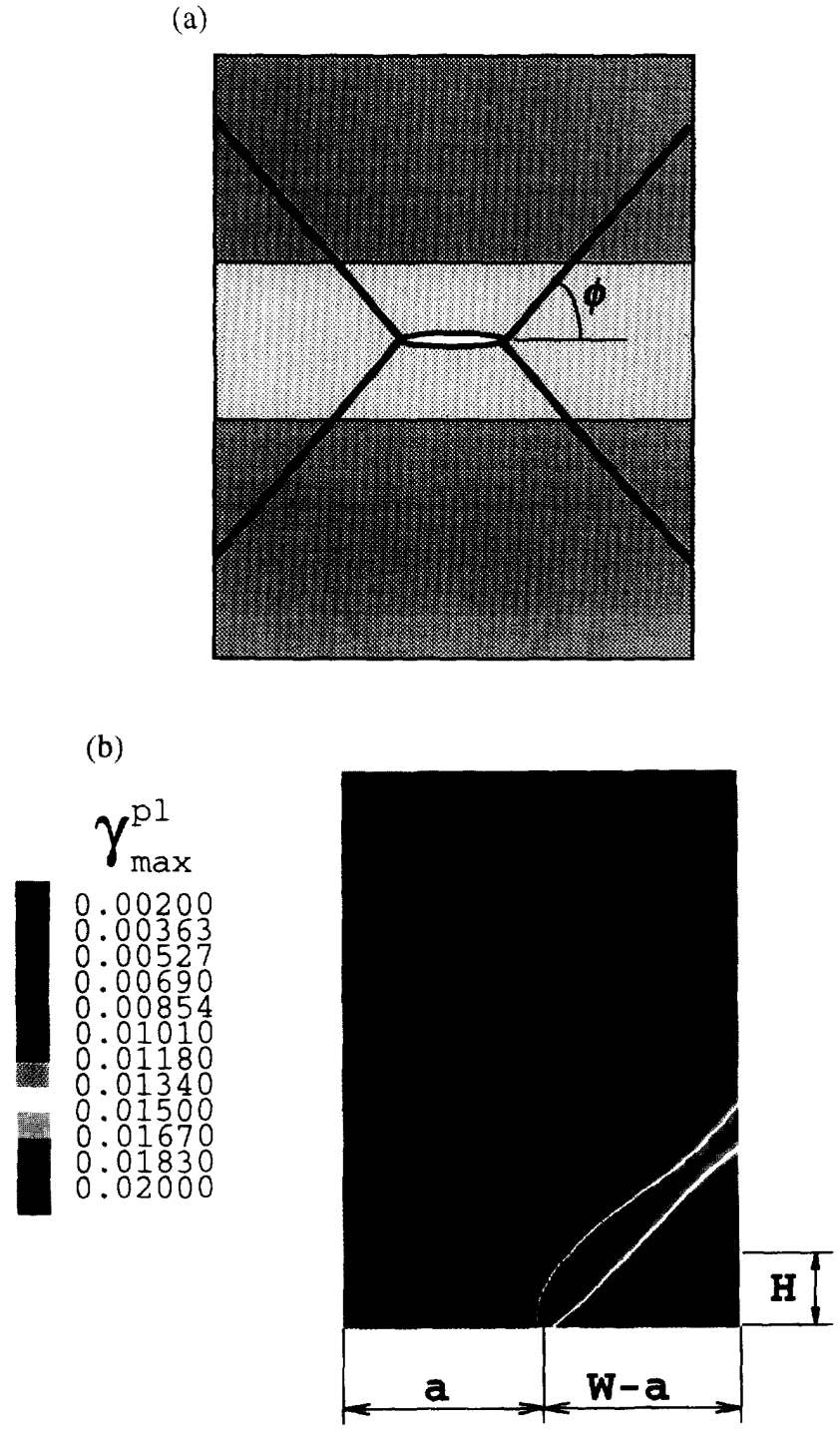

Fig. 10. (a) Penetrating slip-line field for slight undermatching. (b) Contours of maximum shear strain calculated by finite element for slight undermatching.

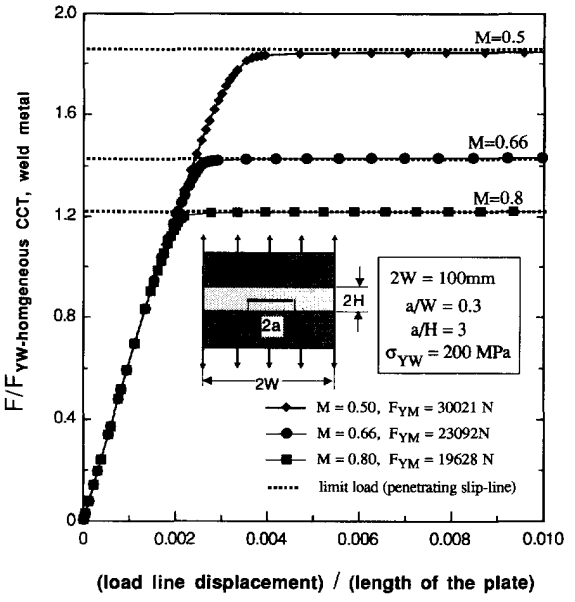

Fig. 11. Comparison between the limit load obtained by slip-line solution and from finite element calculations for slight undermatching.

of homogeneous weld metal. The diagram shows that for vanishing H/W—which in fact means remaining ligament length very large compared to the weld metal strip height—the limit load is governed by the base material yield stress. For finite ratios of H/W, however, dramatic mismatch effects are observed which can be easily quantified using the analytical expressions derived.

4. LIMIT LOAD OF OVERMATCHED TENSION STRUCTURES

First, we assume that both base material and weld metal obey the law of rigid-perfect plasticity, but with different von Mises yield stresses. According to the degree of overmatching and the ratio a/W the general slip-line field has been constructed as shown in Fig. 14. When the yield stress of the weld metal is not much higher than that of the base material, for a given $(W-a)/H$ ratio, the slip-line field has the same form as the penetrating slip-line case in undermatching condition and is shown in Fig. 14(b), which is identical to Fig. 10(a).

On the other hand, if the ratio a/W is small and the yield stress of the weld metal is sufficiently high, plastic flow starts at the corner where the interface intersects the free edge and expands only into the base material as shown in Fig. 14(c). In this case the intensity of the strain singularity at that corner can be stronger than that at the crack tip.

Using the integration like eqn (5) and according to the slip-line fields in Fig. 14(a–c) it is not difficult to calculate the corresponding limit loads. For crack problems the case in Fig. 14(b) is more interesting, and similar to the undermatching condition, the limit load based on the kinematic slip-line field can be expressed as:

$$F_{YM,overmatching,upper\ bound} = \frac{4\sigma_{YW}}{\sqrt{3}}\left[H + \frac{W-a-H}{M}\right] \quad \text{valid for} \frac{W-a}{H} \geqslant 1 \tag{8}$$

which is identical to eqn (6).

From the discussion in the previous section it was mentioned that the kinematically compatible slip-line field leads to an *upper bound solution* of the limit load (Hill, 1951). In other words, eqn (8) may give a higher value as compared with the exact solution. For application it is important to know the difference between this upper bound solution and

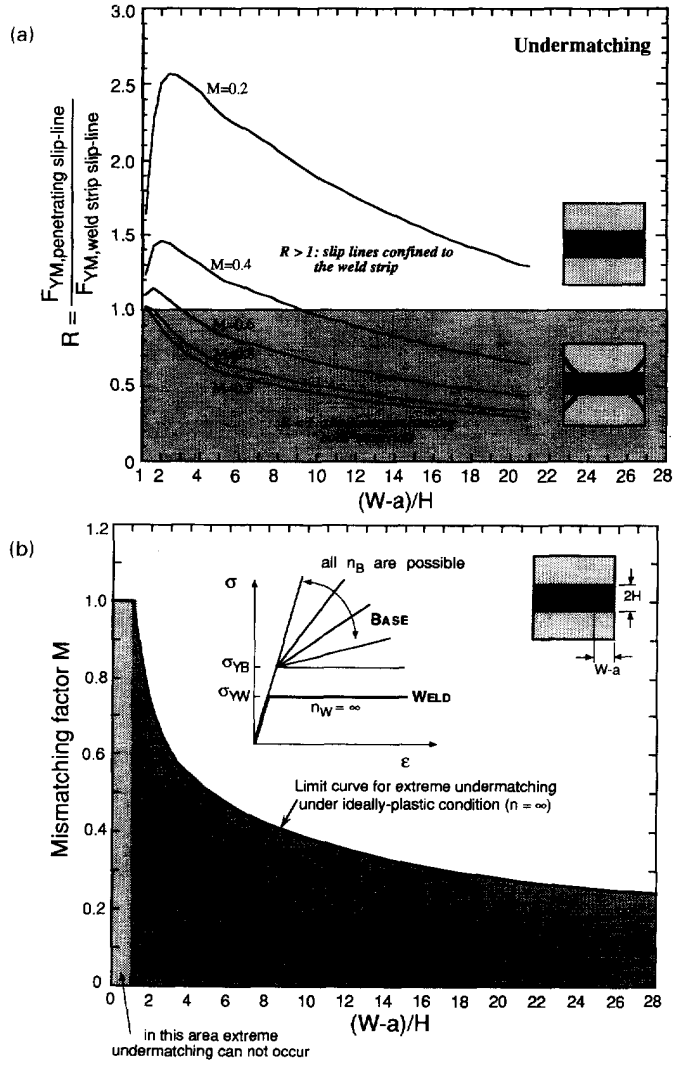

Fig. 12. (a) Relation between the limit load for a penetrating slip-line for slight undermatching and the confined slip-line in the weld strip for extreme undermatching depending on the crack length, strip height and mismatch factor M. (b) Limit curve for extreme undermatching.

the true one, because the upper bound may lead to a non-conservative estimate of the crack driving force.

Opposite the upper bound solution, in the classical theory of plasticity (Hill, 1951, Koiter, 1960) there is another theorem, saying that one may solve any boundary value problem approximately by satisfying only the equilibrium condition, the yielding condition and the force boundary condition. This kind of solution is named a *static equilibrium solution*. The static equilibrium solution leads always to a *lower bound solution* of the limit load. For the structure in Fig. 1 the force boundary condition is

$$\begin{aligned} &\text{at } x_2 = \pm L \quad \sigma_{22} = \sigma_\infty, \sigma_{12} = 0 \\ &\text{at } x_1 = \pm W \quad \sigma_{11} = \sigma_{12} = 0 \end{aligned} \tag{9a}$$

the yielding condition is

$$\begin{aligned} &\text{in the base material:} \quad \sigma_e \leqslant \sigma_{YB} \\ &\text{in the weld material:} \quad \sigma_e \leqslant \sigma_{YW}. \end{aligned} \tag{9b}$$

As a first order approximation, a lower bound solution can be defined as follows:

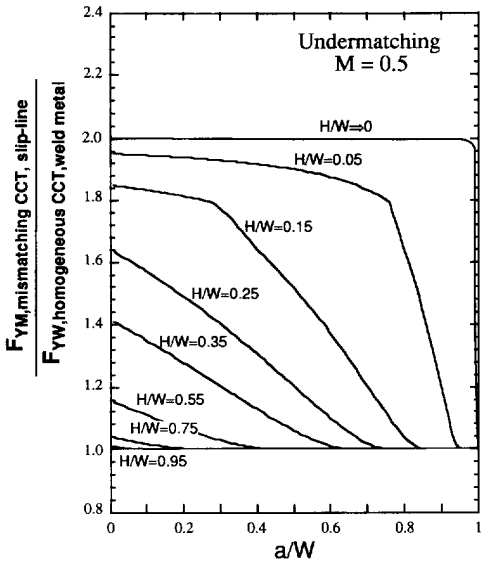

Fig. 13. Overview on the limit load behaviour compared with the homogeneous reference case for a large range of crack length and strip height.

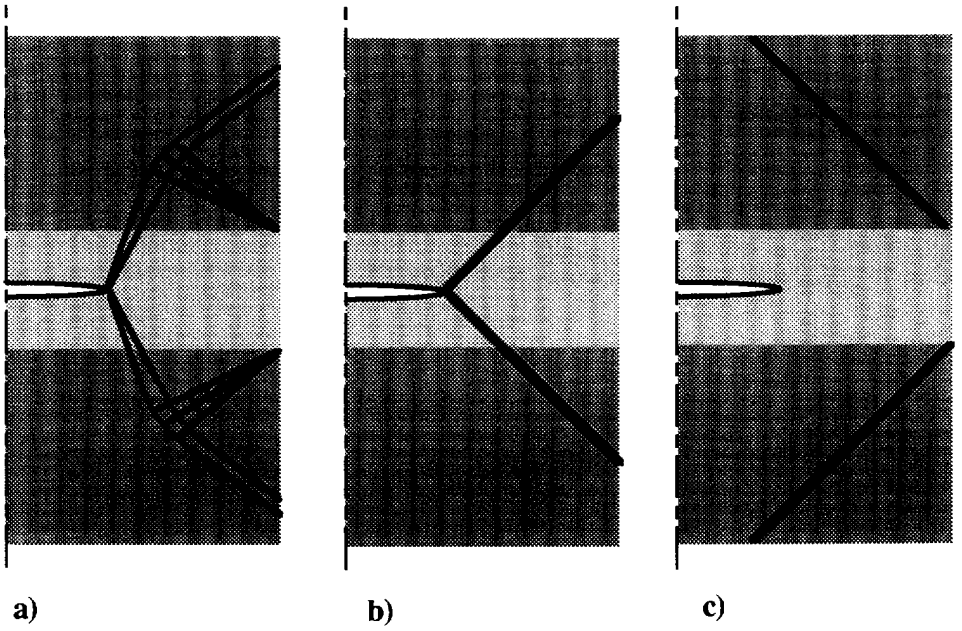

Fig. 14. Slip-lines for overmatching conditions (a) general, (b) slight overmatching, (c) strong overmatching.

$$F_{YM,overmatching,lower\ bound} = \frac{4\sigma_{YW}}{\sqrt{3}}\left[H(1-2g)+\frac{W-a-H}{M}\right] \quad \text{for}\ \frac{W-a}{H} > 1 \qquad (10a)$$

where

$$g = 1-\frac{1}{M}.$$

However, according to the above mentioned theorem we may divide this structure into several blocks as shown in Fig. 15, assuming that in each block the stresses are distributed uniformly so that the conditions in eqns (9a, b) and the equilibrium condition in each block

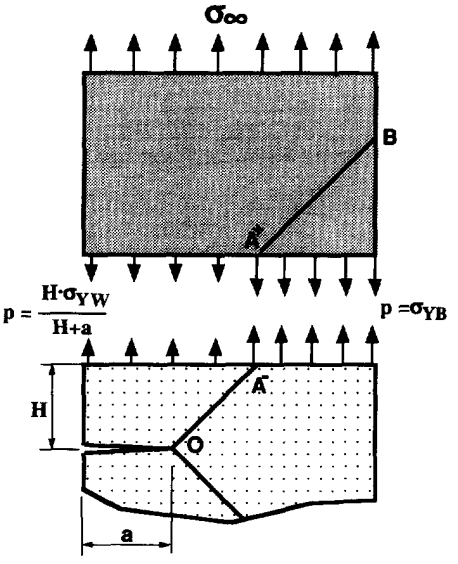

Fig. 15. Determination of the limit load for overmatching using the static lower bound theorem.

and between them can be satisfied. Then from this approximate stress distribution we may derive a limit load which is smaller than or equal to the actual value.

From the stress distribution in Fig. 15 a better expression for the lower bound limit load, as compared with eqn (10a), can be obtained as follows

$$F_{YM,overmatching,lower\ bound} = \frac{4\sigma_{YW}}{\sqrt{3}}\left[H + \frac{W-a-H}{M}\right] \quad \text{for} \frac{W-a}{H} > 1, M \leqslant 1 + \frac{a}{H}. \tag{10b}$$

Comparing this relation with eqn (8) we find when $(W-a)/H > 1$, $(1+a/H) \geqslant M$

$$F_{YM,overmatching,lower\ bound} = F_{YM,overmatching,upper\ bound}$$

which means eqns (8) and (10) are the true solution if the conditions and requirements for them are satisfied.

When $M > (1+a/H)$ the corresponding slip-line fields have been illustrated in Fig. 14(a) or Fig. 14(c). Using a similar procedure we may also obtain the expression for the limit load in these cases. Omitting the deducing process, the resulting relation is

$$F_{YM,overmatching,lower\ bound} = \frac{4\sigma_{YW}}{\sqrt{3}}\left[\frac{W-a-H}{M} + H\right] \quad \text{valid for} \quad M > 1 + \frac{a}{H}. \tag{11}$$

5. CRACK TIP CONSTRAINT

In the foregoing analysis we have already discussed the effect of constraint in a qualitative manner. As noted by O'Dowd and Shih (1991, 1992), the constraint may have an effect on fracture behavior as it may change the stress–strain state around the crack tip. O'Dowd and Shih (1991, 1992) have proposed the J-Q theory to describe the effect of constraint at the crack tip and quantified it by the parameter

$$Q = \left.\frac{\sigma_{\varphi\varphi} - \sigma_{\varphi\varphi HRR}}{\sigma_Y}\right|_{\varphi = 0,\ 1 \leqslant r\sigma_Y/J \leqslant 3} \tag{12}$$

where r, φ denote the polar co-ordinates centred at the crack tip, the subscript HRR represents the stress calculated from the HRR field.

For a perfectly rigid-plastic material, O'Dowd and Shih (1992) have also suggested

$$Q = \left. \frac{\sigma_{\varphi\varphi} - \sigma_{\varphi\varphi,\text{Prandtl}}}{\sigma_Y} \right|_{\varphi = 0,\ 1 \leqslant r\sigma_Y/J \leqslant 3} \tag{13}$$

where the subscript Prandtl denotes the stress component calculated from the solution of the Prandtl field as shown in Fig. 6.

For an extreme undermatching condition we have obtained the slip-line solutions as shown in Fig. 4(a–e) in fully plastic condition, so that these solutions can be used to estimate the stress around the crack tip for this situation, and to calculate the Q factor in an analytical way according to eqn (13), without the need of a point-by-point finite element analysis.

The expressions for Q from slip-line solutions for varying geometric parameters under the condition of extreme undermatching are:

case $(W-a)/H \leqslant 1$

$$Q = -1.81 \tag{14a}$$

case $1 < (W-a)/H \leqslant 1+\pi/2+\sqrt{2}$; the Q factor is fitted by a polynomial in the form

$$Q = -3.2126 + 1.7061\psi - 0.3301\psi^2 + 0.0261\psi^3 \tag{14b}$$

where $\psi = (W-a)/H$

case $1+\pi/2+\sqrt{2} < (W-a)/H$

$$Q = 0. \tag{14c}$$

Figure 16 shows the dependence of the stress distribution ahead of the crack tip, including the position where the parameter Q is determined. One sees that the value of Q

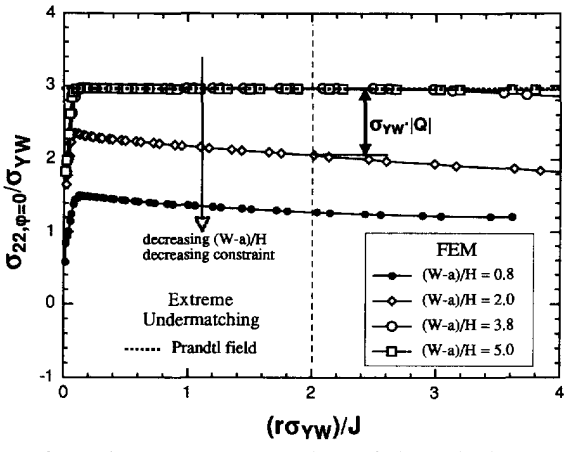

Fig. 16. Distribution of the principal stress σ_{22} near the crack tip on the ligament and the definition of the constraint factor Q.

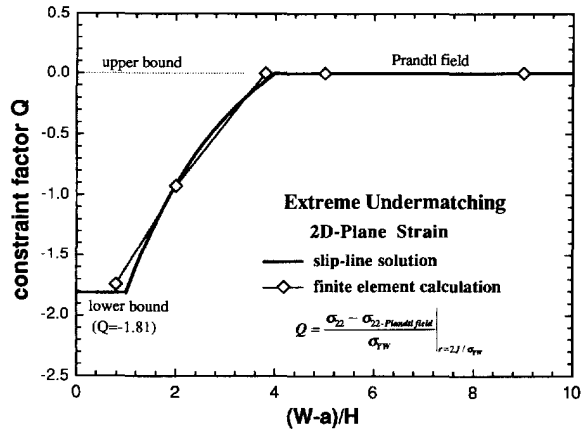

Fig. 17. Comparison of the constraint factor Q obtained by the slip-line solution and finite element calculations for extreme undermatching conditions.

is almost constant in a large range ahead of the crack tip. Figure 17 illustrates Q as determined by eqns (14a–c) and its dependence on geometry in extreme undermatching. In this diagram the corresponding finite element results give the same results.

For overmatching and for slight undermatching, Q takes the value

$$Q = \frac{2}{\sqrt{3}}\left(\frac{1}{M} - 1\right) - 1.81 \tag{15}$$

when the applied load reaches the limit load.

As mentioned in the beginning of this section, extreme undermatching causes an increase in constraint as compared to the homogeneous case which may give rise to an increasing risk of brittle fracture, e.g., to an increase of the temperature of the ductile-to-brittle transition of steels. With the foregoing analysis it is possible to assess this risk quickly.

6. CRACK DRIVING FORCE ESTIMATION WITH ETM-MM

As mentioned in the first section, the prediction of the crack driving force behaviour of a structure with a mismatched welded joint can be done by using the Engineering Treatment Model for Mis-Match (ETM-MM).

The basic construction of the ETM-MM was already introduced in Fig. 2. The key feature of this procedure is using limit load analysis to determine the transition point between local yielding region and fully plastic region. For the tensile loaded centre cracked plate (CCT) with a mismatched welded joint under plane strain condition the limit load has been derived in the present work. Figure 18 shows an overview on the limit load behaviour for under- and overmatching cases as a function of the ligament to weld metal strip height ratio. This diagram shows that for very small ligament ratios ($(W-a)/H < 1$) the weld metal properties dominate whereas for very long ligaments the base material properties take over. The corresponding relations to calculate crack driving force are already listed in eqns (1a–c) using these analytical results, the crack driving force for the mismatched structure shown in Fig. 1 can now be calculated immediately by means of the ETM-MM.

In Fig. 19(a) the behaviour of crack driving force (with δ_5 defined as a crack tip opening displacement) is shown for a group of specimen with varying degrees of overmatching, crack length, and weld strip height. The applied load is normalised by the limit load of the CCT made of homogeneous weld metal. The dependence on the geometry is obvious. Figure 19(b) shows the same data as in Fig. 19(a), but the load is now normalised by the individual limit load and the δ_5 is normalised according to the ETM-MM procedure. All curves,

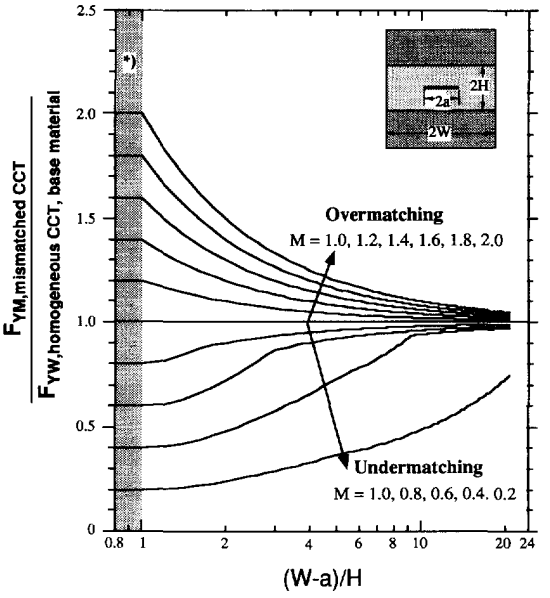

*) in this area: $F_{YM,\text{mismatched CCT}} = F_{YW,\text{homogeneous weld metal CCT}}$

Fig. 18. Limit load for under and overmatching normalized with the limit load of a homogeneous CCT made of base material.

including the ETM-MM prediction, have collapsed to narrow band, in particular in the fully plastic region. Furthermore, Fig. 20 displays the experimental results of three undermatching specimens (Koçak *et al.*, 1988), compared with the prediction of the ETM-MM procedure, i.e., eqns (1a–c). The results shown in Figs 18–20 demonstrate clearly that the ETM-MM procedure is powerful and reliable for failure assessment analyses of mismatch problems.

7. CONCLUSIONS

- A group of slip-line solutions for a mismatched CCT panel with a centred welded joint under plane strain condition has been derived. From these solutions the limit load of this configuration is obtained for different a/W and a/H ratios combined with various degrees of mismatching. The theoretical analysis has been verified by finite element calculations.
- It has been found from the slip-line solution that under the condition of extreme undermatching and $(W-a)/H \geqslant 5.5$ the maximum peak stress does not occur at the crack tip, but ahead of the tip with a distance several times the height of the weld metal strip. This analytic solution agrees with the numerical result in Varias *et al.* (1991). The slip-line solutions indicate that for $(W-a)/H \geqslant 7$ and in the area about 1.5 times weld strip height ahead the crack tip, the value of the maximum principal stress is constant in the transverse direction of the weld metal strip, which agrees with the finite element calculation. Using the slip-line solutions, the value and the position of the maximum stress as well as the hydrostatic stress can be calculated.
- From the slip-line solution the constraint factor Q near the crack tip for a perfectly rigid plastic material in fully plastic condition has been estimated. It shows the same tendency as the results of the respective finite element analyses.
- The analytical results indicate that for extreme undermatching the Q factor is nearly proportional to the ratio of $(W-a)/H$ in the range of $1 \leqslant (W-a)/H \leqslant 4$. When $4 < (W-a)/H$ the Q is constant as derived from the Prandtl field. These findings lead to an important conclusion for engineering applications: for a short crack in long undermatched welded joints, the constraint at the crack tip is higher than for a long crack or for homogeneous conditions. Furthermore, an additional stress peak exists away from the crack tip, which is significantly larger than the respective situation at the crack

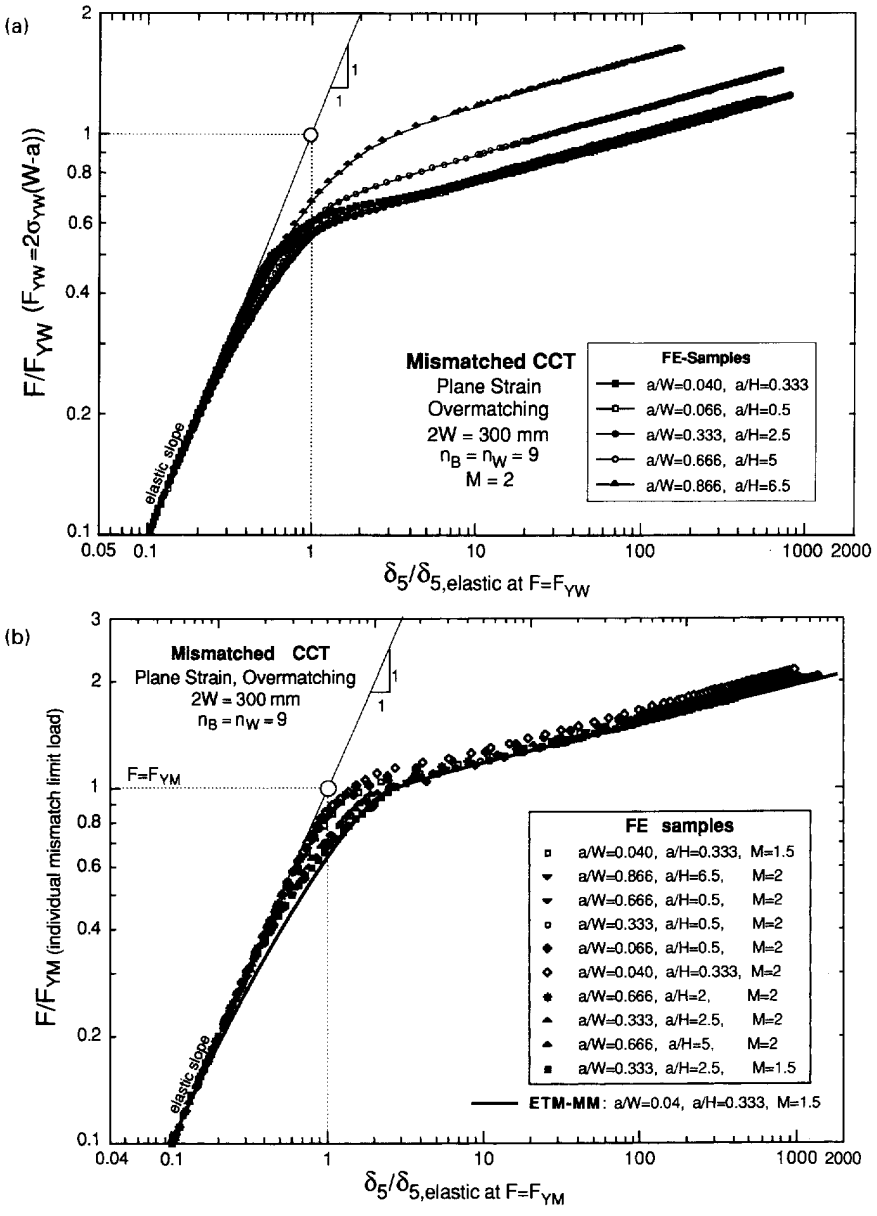

Fig. 19. (a) Load-deformation behaviour for a group of overmatching CCT specimens, the load is normalized with the homogeneous limit load ; finite element results. (b) Load-deformation behaviour for the CCT specimens presented in (a) but here normalized with the mismatched limit load as obtained by the slip-line solutions.

tip and may cause local cleavage cracking in materials prone to cleavage. Therefore, as compared with the homogeneous case, the safety tolerance for these kinds of structures may be reduced as the higher constraint conditions can alter the fracture toughness behaviour (reducing the deformation capacity) or eventually raise the brittle-to-ductile transition temperature.

- The comparison between the crack driving force from the finite element calculation or test results and estimated by the ETM-MM procedure shows that this procedure is powerful for estimating the crack driving force or load-deformation capacity of cracked structures.

Further work on mismatch effects in other geometries is in progress. It is mainly focused on slip-line solutions for bending configurations (Hao *et al.*, 1994b) and also for the plane stress condition as well as on the three-dimensional behaviour of CCT panels

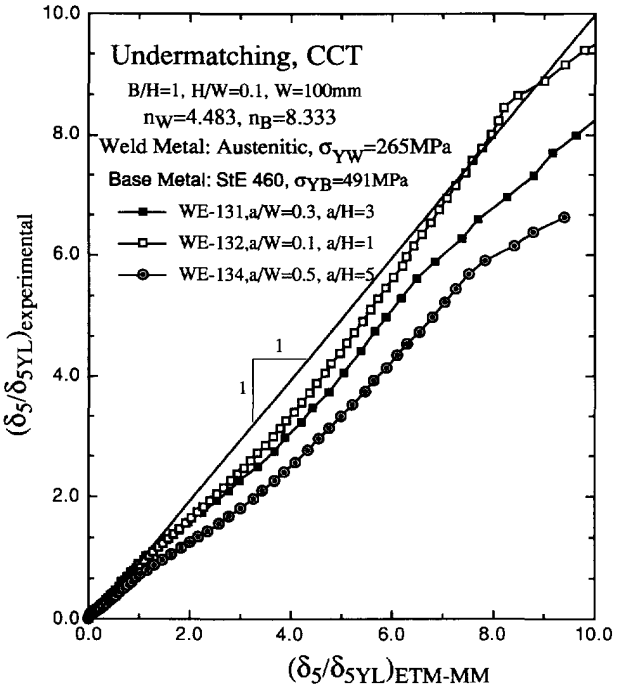

Fig. 20. Comparison of experimental results for the crack driving force (denoted here as δ_5) and the prediction with the new ETM-MM.

(Hao *et al.*, 1994c). The effect of strain hardening on the relevance of slip-line solutions will also be looked at.

Acknowledgements—The authors gratefully acknowledge the financial support by the German Science Foundation (Deutsche Forschungsgemeinschaft, Sonderforschungsbereich 371). The test data of undermatched CCT specimens were provided by Dr M. Koçak, the authors want to also express their appreciation for this assistance.

REFERENCES

Denys, R. (1991). Provisional definitive statement on the significance of over and undermatching weld metal strength. *IIW-Doc. X*-1222-91.

Dewhurst, P. and Collins, I. F. (1973). A matrix technique for constructing slip-line field solutions to a class of plane strain plasticity problems. *Int. J. Num. Meth. Engng* **7**, 357–378.

Dong, P. and Gordon, J. R. (1990). The effect of undermatching on fracture prediction models. *Welding* 90 (ed. M. Koçak), IITT-International, France.

Dowling, A. R. and Townley, C. H. A. (1975). The effects of defects on structural failure: a two-criteria approach. *Int. J. Pressure Vessel and Piping* **3**, 77–137.

Geiringer, H. (1930). *Proc. 3rd Int. Cong. App. Mech.* Stockholm, Vol. 2, p. 185.

Gordon, J. R. and Wang, Y.-Y. (1993). The effect of weld metal mis-match on fracture toughness testing and analysis procedures. *Mis-Matching of Welds, ESIS* 17, *Proceedings of Mis'match* 93, May, 1993, Reinstof, Germany, Mechanical Engineering Publications, London, pp. 351–368.

Hao, S., Cornec, A. and Schwalbe, K.-H. (1991). Anwendung des Engineering Treatment Model (ETM) auf Schweißverbindungen: Mittenrißschreibe (CCT) mit einem idealisierten Scheibenstreifen quer zur Beanspruchung. GKSS technical note *GKSS/WW*/91/13.

Hao, S., Cornec, A. and Schwalbe, K.-H. (1994a). On the crack driving force and constraint state in a mismatched welded plate under tension. *Mis-Matching of Welds, ESIS* 17, *Proceedings of Mis'match* 93, May, 1993, Reinstof, Germany, Mechanical Engineering Publications, London, pp. 561–571.

Hao, S., Cornec, A. and Schwalbe, K.-H. (1994b). On the slip-line solution for bending specimen with mismatched welded joint, *GKSS Technical Note*.

Hao, S., Cornec, A. and Schwalbe, K.-H. (1994c). Investigation on the effect of thickness on the constraint state and limit loads of the mismatched welds—2D and 3D analyses. *IIW Doc. X-F*-015-94, presented at the Intermediate Meeting of the IIW Sub-Commission X-F, 28–29 April 1994, Paris.

Hao, S., Cornec, A. and Schwalbe, K.-H. (1994d). On the crack driving force and fracture resistance of mismatched weldments. *Proc. of ECF*10, vol. 2, pp. 1117–1123.

Hill, R. (1951). *The Mathematical Theory of Plasticity*, Oxford.

Hutchinson, J. (1968). Plastic stress and strain fields at a crack tip. *J. Mech. Phys. Solids* **16**, 337–347.

Joch, J., Ainsworth, R. A. and Hyde, T. H. (1993). Limit load and *J*-estimates for idealised problems of deeply cracked welded joints in plane strain bending and tension. *Fatigue Fracture Engng Mat. Struct.* **16**, 1061–1079.

Kirk, M., Koppenhoefer, K. C. and Shih, C. F. (1991). Effect of constraint on specimen dimensions needed to obtain structurally relevant toughness measures. *ASTM STP* 1171, 79–103.
Kirk, M. T. and Dodds, R. H. (1992). Experimental *J* estimation formulas for single edge notch bend specimens containing mismatched weld. *Proceedings of the 11th Conf. on Offshore Mechanics and Arctic Engineering*, ASME, pp. 439–448.
Koiter, W. (1980). General theorems for elastic–plastic solids. In *Progress on Solid Mechanics*, Vol. 1 (eds Snedden and Hill).
Koçak, M., Schwalbe, K.-H., Chen, L. and Gnirss, G. (1988). Effects of notch position and weld metal matching on CTOD of HAZ. *Proc. of the Int. Conf. on Weld Failure*, TWI, p. 7.
Koçak, M., Knaack, J. and Schwalbe, K.-H. (1990). Fracture behaviour of undermatched weld joint. In *Proc. of the 9th Int. Conf. on Offshore Mech. and Arctic Engng, ASME*, Houston, Texas, pp. 453–459.
Kumar, V., German, M. D. and Shih, C. F. (1931) An engineering approach for elastic–plastic fracture analysis. *EPRI Report NP*-1931.
O'Dowd and Shih, F. (1991). Family of crack-tip fields characterised by a triaxiality parameter: part I—structure of fields. *J. Mech. Phys. Solids* **39,** 337–347.
O'Dowd and Shih, F. (1992). Family of crack-tip fields characterised by a triaxiality parameter: part I—fracture application/ *J. Mech. Phys. Solids* **40,** 939–963.
Petrovski, B. and Koçak, M. (1994). Evaluation of the fracture behaviour of strength mis-matched steel weld joints with surfaced tensile panels and SENB specimens. *Mis-Matching of Welds, ESIS* 17, *Proceedings of Mis'match* 93, May, 1993, Reinstof, Germany, Mechanical Engineering Publications, London, pp. 511–530.
Prandtl, L. (1923). Anwendungsbeispiele zu einem Henckyschen Satz über das plastische Gleichgewicht. *Z. Angew. Math. Mechanik* **3,** 401–406.
Prager, W. (1953). General discussion of the slip line field in plane plastic flow. *Trans. Royal Institute of Tech.* **65.**
Schwalbe, K.-H. (1992). Effect of weld metal mis-match on toughness requirements: same simple analytical considerations using the Engineering Treatment Model (ETM). *Int. J. Fract.* **56,** 257–277.
Schwalbe, K.-H. and Cornec, A. (1991). The engineering treatment model (ETM) and its practical application. *Fatigue Fract. Engng Mat. Struct.*, **14,** 405–412.
Schwalbe, K.-H., Hao, S. and Cornec, A. (1994). ETM-MM—the engineering treatment model for mis-matched welded joints. *Mis-Matching of Welds, ESIS* 17, *Proceedings of Mis'match* 93, May 1993, Reinstof, Germany, Mechanical Engineering Publications, London, pp. 539–560.
Thaulow, C., Paauw, A. J., Hauge, M., Toyoda, M. and Minami, F. (1994). Fracture property of HAZ-notched weld joint with mechanical mis-matching—part II. Effect of local mechanical mis-matching on fracture initiation in steel weldment. *Mis-Matching of Welds, ESIS* 17, *Proceedings of Mis'match* 93, May, 1993, Reinstof, Germany, Mechanical Engineering Publications, London, pp. 417–432.
Toyoda, M., Minami, F., Ruggieri, C., Thaulow, C. and Hauge, M. (1994). Fracture property of NAZ-notched weld joint with mechanical mis-matching—part I. Analysis of strength mis-matching of welds on fracture initiation resistance of HAZ-notched joint. *Mis-Matching of Welds, ESIS* 17, *Proceedings of Mis'match* 93, May, 1993, Reinstof, Germany, Mechanical Engineering Publications, London, pp. 399–417.
Varias, A. G., Suo, Z. and Shih, C. F. (1991). *J. Mech. Phys. Solids* **39,** 963.
Zhang, J. X., Shi, Y. W. and Tu, M. J. (1989). Studies on the fracture mechanics parameters of weldment with mechanical heterogeneity. *Engng Fracture Mech.* **34,** 1041–1050.

APPENDIX 1: SLIP-LINE FIELDS FOR EXTREME UNDERMATCHING

Case 1*a*: $(W-a)/H \leqslant 1$ (Fig. 4a)

In this case the slip-line field for undermatching is the same as for the homogeneous case. The limit load is

$$F_{YM,\text{slip-line weld strip}} = \frac{4\sigma_{YW}}{\sqrt{3}}(W-a) \tag{A1-1}$$

and the maximum principal stress at the crack tip is

$$\sigma_{yy}|_{\text{crack tip}} = \frac{2\sigma_{YW}}{\sqrt{3}} \tag{A1-2}$$

Case 1*b*: $1 < (W-a)/H \leqslant 1+\pi/2+\sqrt{2}$ (Fig. 4b)

The slip-line field is constructed by a fan-shaped field followed by a cycloid field, see Fig. 4b. The transition field between these basic slip-line systems was omitted. The slip-line family in the cycloid field is described as follows

$$\alpha-\text{line}: \frac{x}{h} = \sin^{-1}\left(\frac{y}{h}\right) - \sqrt{1-\frac{y^2}{h^2}} + C \tag{A1-3a}$$

$$\beta-\text{line}: \frac{x}{h} = -\sin^{-1}\left(\frac{y}{h}\right) - \sqrt{1-\frac{y^2}{h^2}} + C \tag{A1-3b}$$

where the origin of the co-ordinate system $\{x_1, x_2\}$ is at the crack tip, and $h \neq H$, which is determined by the equilibrium condition.

It is known that the slip-line radiating out from the crack tip must be inclined to the horizonal axis by 45 degrees because of the symmetry, and the resultant force in horizontal direction on the slip line NPO in Fig. 4(b)

equals zero as the plate edge is traction-free. From these requirements and the stress connection condition at point P we can determine the parameter h in eqns (A1-3) and the angle between the line NP and the horizontal line. Then the whole slip-line field on the ligament is determined according to the process in Hill (1951). From the solution the maximum principle stress at the crack tip and the limit load are fitted by polynomials as

$$\sigma_{22}|_{crack\ tip} = \frac{\sigma_{YW}}{\sqrt{3}}[-0.423+2.956\psi-0.571\psi^2+0.0452\psi^3] \tag{A1-4}$$

and

$$F_{YM,slip\text{-}line\ weld\ strip} = \frac{4\sigma_{YW}(W-a)}{\sqrt{3}}[0.915-0.0276\psi+0.1185\psi^2-0.0165\psi^3] \tag{A1-5}$$

with $\psi = (W-a)/H$.

Case 1c: $1+\pi/2+\sqrt{2} < (W-a)/H \leqslant 1+\pi/2+2\sqrt{2}$ (Fig. 4c)

The slip-line field is constructed by the fan-shaped field at plate edge, followed by the cycloid field, and the Prandtl field at the crack tip, as well as somewhere transition fields in-between. The cycloid fields are described by

$$\alpha\text{-line}: \frac{x}{h} = \sin^{-1}\left(\frac{y}{h}\right) - \sqrt{1-\frac{y^2}{h^2}} + C; \quad \beta\text{-line}: \frac{x}{h} = -\sin^{-1}\left(\frac{y}{h}\right) - \sqrt{1-\frac{y^2}{h^2}} + C. \tag{A1-6}$$

As at the crack tip the Prandtl field solution governs the stress–strain field, the maximum principal stress at the crack tip is

$$\sigma_{22}|_{crack\ tip} = \frac{(2+\pi)\sigma_{YW}}{\sqrt{3}} \tag{A1-7}$$

the limit load fitted by a polynomial is given by

$$F_{YM,slip\text{-}line\ weld\ strip} = \frac{4\sigma_{YW}(W-a)}{\sqrt{3}}[-0.637+1.0333\psi-0.147\psi^2+0.0079\psi^3] \tag{A1-8}$$

where ψ is defined in eqn (A1-5).

Case 1d: $1+\pi/2+2\sqrt{2} < (W-a)/H \leqslant 3.88+2\pi+\sqrt{2}$ (Fig. 4d)

As shown in Fig. 4(d), a new slip-line field, denoted as CDEHG, evolves at the right side of the Prandtl field. Using the numerical method (Hill, 1951, Dewhurst and Collins, 1973) it is not difficult to derive the α–β network, according to the stress connection conditions on the arc CDE and the tangent condition of slip-line on the interface. To give an overview of the slip-line field in this area, we may use the following relation to describe the β family of slip-lines approximately

$$\beta\text{-lines}: \frac{x}{H} = \sqrt{1-\frac{y^2}{H^2}} + C. \tag{A1-9}$$

These slip-lines are tangential to the interface between base and weld material and parallel to the arc DC. Taking into account the orthogonal condition we can determine the α family in CDH from eqn (A1-9) nearly, for example, the line DH. In the zone DEGH, according to the Henky's theorem (Hill, 1951), all lines in the β family are straight lines as the line DE is straight. The slope of the line DH is known, so that the slip-line field in DEGH is finally determined. The slip-line field in zone EGF is similar to the cycloid field in Fig. 4b but the cycloids are described by

$$\frac{x}{h} = \mp\sin^{-1}\left(\frac{y}{h}\right) + \sqrt{1-\frac{y^2}{h^2}} + C \tag{A1-10}$$

with $h \neq H$.

Combining the stress continuity condition at the point F and the traction-free condition at the edge of the plate one may obtain h in eqn (A1-10) and the position of F, then the whole slip-line field in the ligament is determined. By using the approximate expression (A1-9) and omitting the transition zone near arcs PK, EG, the deviation of the calculated stresses, as compared with the numerical solution, is less than 3% (refer to Appendix 2).

The maximum principal stress at the crack tip is the same as the one in the Case 1c:

$$\sigma_{22}|_{crack\ tip} = \frac{(2+\pi)\sigma_{YW}}{\sqrt{3}}. \tag{A1-11}$$

The limit load fitted by a polynomial is

$$F_{YM,slip\text{-}line\ weld\ strip} = \frac{4\sigma_{YW}(W-a)}{\sqrt{3}}[1.693-0.0497\psi+0.02\psi^2-0.00076\psi^3] \tag{A1-12}$$

where ψ is defined in eqn (A1-5).

Case 1*e*: $3.88+2\pi+\sqrt{2}<(W-a)/H$ (Fig. 4e)

The structure of the slip-line field is similar to the Case 1d, however both the field DEGH and field EFG expand to the interface of the two materials. The cycloid field EFG, similar to eqn (A1-10), is described by

$$\frac{x}{H} = \mp\sin^{-1}\left(\frac{y}{H}\right)\pm\sqrt{1-\frac{y^2}{H^2}}+C. \tag{A1-13}$$

The maximum principal stress at the crack tip is given by

$$\sigma_{22}|_{crack\ tip} = \frac{(2+\pi)\sigma_{YW}}{\sqrt{3}}. \tag{A1-14}$$

The limit load fitted by a polynomial is

$$F_{YM,slip\text{-}line\ weld\ strip} = \frac{4\sigma_{YW}(W-a)}{\sqrt{3}}[1.1896+0.12264\psi] \tag{A1-15}$$

where ψ is defined in eqn (A1-5).

APPENDIX 2: TRANSITION ZONE BETWEEN BASIC SLIP-LINE SOLUTIONS

As indicated previously, to avoid tedious numerical analyses we may omit the transition zone surrounding the arc EG and PK in Fig. 4(b–e) to obtain a simple analytical solution. How large is the deviation caused by this simplification? This question is still open. Because of the limited space, in the following we shall discuss only one typical example: the effect of this simplification to the Case 1d in Appendix 1, that is, in the area near the arc PK at the right side of the slip-line field shown in Fig. 4(d).

In this case we may first let the stress continuity condition of the α-line on FPN be satisfied without transition zone, but the β-line PK, the boundary of the fan-shaped field KNP, is not exactly coincident with the cycloid field FKP. The stress discontinuity is zero at point P but increases along the arc PK. It reaches its maximum value at point K. From the cycloid field the stress in vertical direction at point K is:

$$\sigma_{22,K}|_{cycloid\text{-}field} = \frac{\sigma_{YW}}{\sqrt{3}}\left[2-\sqrt{2}+\frac{\pi}{2}\right]. \tag{A2-1}$$

The same stress component calculated from the fan-shaped field at point K is

$$\sigma_{22,K}|_{fan\text{-}shaped\text{-}field} = \frac{2\sigma_{YW}}{\sqrt{3}}. \tag{A2-2}$$

The fractional deviation between both is

$$\frac{\sigma_{22,K}|_{cycloid\text{-}field}-\sigma_{22,K}|_{fan\text{-}shaped\text{-}field}}{\sigma_{22,K}|_{fan\text{-}shaped=field}} = \frac{\pi/2-\sqrt{2}}{2} \approx 0.047. \tag{A2-3}$$

APPENDIX 3: LIMIT LOAD FOR PENETRATING SLIP-LINE FIELD

From Fig. 10(a) and the previous discussion in this paper it was shown that the slip-line includes an angle of 45° with the horizontal axis. According to the traction-free condition at the edge of the plate, σ_{22} on the slip-line must be $2\sigma_{YB}/\sqrt{3}$, where σ_{YB} denotes the yield stress of the base material. According to the stress connection conditions introduced in Appendix 4, eqn (A4-4a), an expression of limit load can be defined as

$$F_{YM,overmatching,lower\ bound} = \frac{4\sigma_{YW}}{\sqrt{3}}\left[H\left(\frac{2}{M}-1\right)+\frac{W-a-H}{M}\right]. \tag{A3-1a}$$

If we assume that there is a stress jump on the slip-line at the interface and the yielding condition must be satisfied on the slip-line in the weld metal, as illustrated in Fig. 15 for both over- and undermatching, σ_{22} on the slip-line in the weld metal must be $2\sigma_{YW}/\sqrt{3}$. The limit load in this case is

$$F_{YM,penetrating\ slip\text{-}line} = \frac{4\sigma_{YW}}{\sqrt{3}}\left[H+\frac{W-a-H}{M}\right]. \tag{A3-1b}$$

The finite element analysis indicates that eqn (A3-1b) is nearer reality.

APPENDIX 4: DISCONTINUITY OF SLIP-LINES CROSSING THE INTERFACE BOUNDARY

In Fig. A1 the line L is an interface and the superscript "+" or "−" represents the quantity in either material. Consider an infinitesimal element on L, from the stress continuity condition we have:

$$\sigma_n^+ = \sigma_n^- ; \quad \tau_n^+ = \tau_n^- \tag{A4-1}$$

and it is allowed to set

$$\sigma_t^+ \neq \sigma_t^- . \tag{A4-2}$$

From the equilibrium condition at both materials we have the relation

$$\sigma_n^+ = \sigma_m^+ - k^+ \sin 2(\theta^+ - \zeta) ; \quad \tau_n^+ = k^+ \cos 2(\theta^+ - \zeta) \tag{A4-3a}$$

and

$$\sigma_n^- = \sigma_m^- - k^- \sin 2(\theta^- - \zeta) ; \quad \tau_n^- = k^- \cos 2(\theta^- - \zeta) \tag{A4-3b}$$

where θ denotes the helix angle of an α family slip-line, σ_m is the mean stress, k represents the shear yield strength of the material and ζ is the angle between the normal vector of the interface and the x_1-coordinate (see Fig. A1).

Substituting eqns (A4-3a, b) in eqn (A4-1) the following conditions of the stress components for a slip-line field across an interface can be obtained (Prager, 1953):

$$\sigma_m^+ - k^+ \sin 2(\theta^+ - \zeta) = \sigma_m^- - k^- \sin 2(\theta^- - \zeta) \tag{A4-4a}$$

and

$$k^- \cos 2(\theta^+ - \zeta) = k^- \cos 2(\theta^- - \zeta). \tag{A4-4b}$$

Then we consider the displacement continuity condition of a slip-line field across an interface. Looking at Fig. A1 at point A on L the displacement continuity condition must be satisfied if the interface does not coincide with a slip-line:

$$v_1^+ |_A = v_1^- |_A ; \quad v_2^+ |_A = v_2^- |_A \tag{A4-5}$$

where v_1, v_2 represent the velocity (rate of displacement) in x_1 and x_2 directions, respectively.

If the interaction coincides with a slip-line, the displacement continuity condition degenerates to:

$$v_2^+ |_A = v_2^- |_A . \tag{A4-5'}$$

Obviously at any point on the interface, for example, at point B on L in Fig. A1, the continuity condition must be satisfied. From the well-known relation suggested by Geiringer (1930) it is

$$\text{on an } \alpha\text{-line}: \mathrm{d}v_\alpha = v_\beta \, \mathrm{d}\theta$$

$$\text{on a } \beta\text{-line}: \mathrm{d}v_\beta = v_\alpha \, \mathrm{d}\theta$$

where θ is the angle between the α slip-line and horizontal axis, the subscripts α, β represent the velocity (rate of displacement) in α line and ν line directions. From Geiringer's relation one can obtain directly the following sufficient condition for the displacement continuity of a slip-line field across an interface:

$$\theta_B^+ - \theta_A^+ = \theta_B^- - \theta_A^- . \tag{A4-6}$$

When the slip-line field degenerates into a single slip line, the infinitesimal element on L (Fig. A1) vanishes, so that in this case only eqn (A4-5) holds as the necessary and sufficient condition.

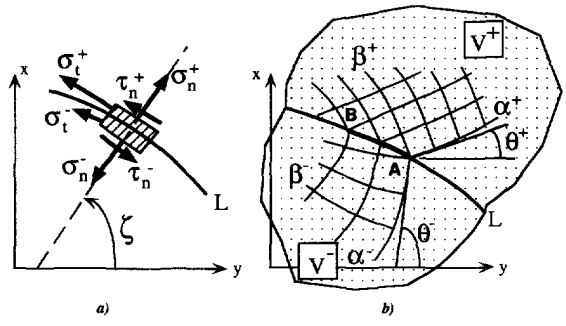

Fig. A1. Graphical explanation of the slip-line discontinuity at an interface.

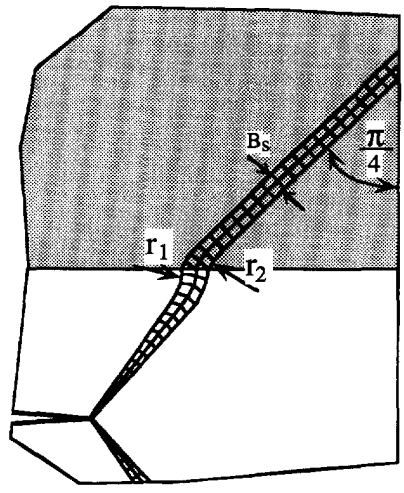

Fig. A2. A general solution of the slip-line field for slight over- or undermatching.

It is easy to prove that all variation principles, derived for a homogeneous body that may contain stress discontinuities, are also applicable to a solid body composed of two materials joined by an interface, if on the interface there is no debonding. This is because in this case an interface does neither generate new boundary conditions or exhaust extra energy, the virtual work rate principle for the body, for example, as shown in Fig. A1, is

$$\int_{V^+} \sigma_{ij}\dot{\varepsilon}_{ij}\,\mathrm{d}V^+ + \int_{V^-} \sigma_{ij}\dot{\varepsilon}_{ij}\,\mathrm{d}V^- = \int_{LS^+} T_{Li}^- v_{Li}^+\,\mathrm{d}S + \int_{LS^-} T_{Li}^- v_{Li}^-\,\mathrm{d}S + \int_S T_i v_i\,\mathrm{d}S \tag{A4-7}$$

where S denotes the boundary, LS^+ and LS^- are the interface, corresponding to V^+, V^-, respectively. Obviously, when there is no debonding:

$$T_{Li}^+ = -T_{Li}^- = T_L; \quad v_{Li}^+ - v_{Li}^- = [v_{Li}]$$

and

$$\int_{S^-} T_{Li}^+ v_{Li}^+\,\mathrm{d}S + \int_{S^-} T_{Li} v_{Li}^-\,\mathrm{d}S = \int_{S^-} T_{Li}[v_{Li}]\,\mathrm{d}S.$$

The virtual work rate equation becomes

$$\int_{V^-} + V^+ \sigma_{ij}\dot{\varepsilon}_{ij}\,\mathrm{d}V = \int_S T_i v_i\,\mathrm{d}S + \int_{LA} T_{Li}[v_{Li}]\,\mathrm{d}S \tag{A4-8}$$

which is the same as in the homogeneous case with some local displacement discontinuities, such as slip-lines.

Now we go back to the configuration in Fig. 10(a), where

$$\zeta = \frac{\pi}{2} \quad k^+ = \frac{\sigma_{YB}}{\sqrt{3}} \quad k^- = \frac{\sigma_{YW}}{\sqrt{3}}. \tag{A4-9}$$

A general form of slip-line field as shown in Fig. A2 can be constructed. Using eqns (A4-4a, b) and (A4-6) one may determine the angles θ^+ and θ^- and $\Delta\theta$ at the interface. However, it is obvious that smaller radii r_1, r_2 in Fig. 22 and narrower slip-bands (smaller B_S) lead to less plastic energy dissipation and correspond to a lower limit load. The limiting case is that r_1, r_2 and B_S approach zero, so that the slip-line field degenerates into the field shown in Fig. 10(a) and the corresponding limit load is given by eqn (A3-1).

We can also investigate this problem in another way. Considering the upper quarter of the plate in Fig. 7 and separating it into two parts, one may obtain a solution as shown in Fig. 15, which satisfies the global equilibrium condition and displacement compatibility condition, but for undermatching in some local areas the yielding condition may not be satisfied, so that in this case an upper bound solution of the limit load of the structure, as expressed in eqn (A3-1), can be derived from the slip-line field in Fig. 10(a).